

Stephen F. Austin State University

SFA ScholarWorks

Electronic Theses and Dissertations

5-2017

Basement and Cover Structural Analysis Along the Eagle River Gorge, Sawatch Range, Colorado

Kaitlin Lee Askelson

Stephen F Austin State University, kaitlin.askelson@gmail.com

Follow this and additional works at: <https://scholarworks.sfasu.edu/etds>



Part of the [Geology Commons](#), and the [Tectonics and Structure Commons](#)

[Tell us](#) how this article helped you.

Repository Citation

Askelson, Kaitlin Lee, "Basement and Cover Structural Analysis Along the Eagle River Gorge, Sawatch Range, Colorado" (2017). *Electronic Theses and Dissertations*. 92.

<https://scholarworks.sfasu.edu/etds/92>

This Thesis is brought to you for free and open access by SFA ScholarWorks. It has been accepted for inclusion in Electronic Theses and Dissertations by an authorized administrator of SFA ScholarWorks. For more information, please contact cdsscholarworks@sfasu.edu.

Basement and Cover Structural Analysis Along the Eagle River Gorge, Sawatch Range, Colorado

Creative Commons License



This work is licensed under a [Creative Commons Attribution-Noncommercial-No Derivative Works 4.0 License](https://creativecommons.org/licenses/by-nc-nd/4.0/).

BASEMENT AND COVER STRUCTURAL ANALYSIS ALONG THE
EAGLE RIVER GORGE, SAWATCH RANGE, COLORADO

By

Kaitlin Lee Askelson, Bachelor of Science

Presented to the Faculty of the Graduate School of
Stephen F. Austin State University

In Partial Fulfillment

Of the Requirements

For the Degree of Master of Science

STEPHEN F. AUSTIN STATE UNIVERSITY

May, 2017

BASEMENT AND COVER STRUCTURAL ANALYSIS ALONG THE EAGLE
RIVER GORGE, SAWATCH RANGE, COLORADO

By

Kaitlin Lee Askelson, Bachelor of Science

APPROVED:

Dr. Chris Barker, Thesis Director

Dr. Melinda Faulkner, Committee Member

Dr. Joseph Musser, Committee Member

Dr. Liane Stevens, Committee Member

Dr. Joseph Allen, Committee Member

Richard Berry, D.M.A.
Dean of the Graduate School

ABSTRACT

The Sawatch Range within the Rocky Mountains of central Colorado exposes Paleoproterozoic basement and overlying Paleozoic sedimentary rocks with a complex history of ductile and brittle deformation.

The goal of this study is to conduct analyses of brittle structures that occur in the basement and cover units to determine geometric relationships between the structures, provide a detailed description of structures and refine a geologic history for structures along the basement-cover contact in the northeastern Sawatch Range along the Eagle River canyon and U.S. Highway 24 from Red Cliff to Gilman, Colorado. Paleoproterozoic basement rocks include the Cross Creek granite, diorites, and gneisses. The basement rocks are nonconformably overlain by the late Cambrian age Sawatch Formation.

Measurements of 60 fault planes were recorded and of those, 36 exhibited dip-slip or strike-slip movement. Faults exhibited an average northeast strike throughout the study area. Measurements of 151 joint planes were taken throughout the study area and joints exhibit a northwest strike on average. Structural trends observed in this area represent different orientations that were created by multiple deformational events throughout geologic history. These deformational events include the accretion of volcanic island arcs and continental crust onto Laurentia, Ancestral Rocky Mountain Uplift and the Laramide orogeny.

ACKNOWLEDGMENTS

I would like to thank Dr. Chris Barker for advising my research and I would also like to thank the members of my committee: Dr. Melinda Faulkner, Dr. Liane Stevens, Dr. Joseph Musser of the Physics Department and Dr. Joseph Allen at Concord University, in West Virginia. Thank you for providing additional guidance and being additional readers of this thesis. I would not have been able to complete this work without the support of my family and friends; their support of my work allowed me to reach my goals for this research. Without these people, such an effort would not have been possible and I am truly grateful.

TABLE OF CONTENTS

Abstract	p. i
Acknowledgments	p. ii
Chapter 1 Introduction	p. 1
Chapter 2 Geologic Setting and Previous Works	p. 6
Regional Geology and Structure	p. 6
Tectonic Evolution and Stratigraphy of the Central Rocky Mountains	p. 11
Precambrian Geology of Southwest Laurentia	p. 11
Introduction: Island Arc Accretion	p. 11
Yavapai Province	p. 14
Mazatzal Province	p. 14
Precambrian Shear Zones of Colorado	p. 15
Paleoproterozoic Rocks in the Study Area: Cross Creek Granite, Diorite and Gneiss	p. 17
Paleozoic Geology	p. 19
Paleozoic Rocks in the Thesis Area: Cambrian Sawatch Sandstone	p. 19
Ancestral Rocky Mountains	p. 20
Mesozoic Geology and the Laramide Orogeny	p. 22
Cenozoic Geology: Igneous Activity and Rio Grande Rifting	p. 24
Colorado Mineral Belt	p. 27
Mining History	p. 29
Chapter 3 Methods and Field Observations	p. 31
Introduction	p. 31
Description of Rock Units	p. 35
Introduction	p. 35

Cross Creek Granite	p. 35
Diorite	p. 36
Gneiss	p. 37
Pegmatites	p. 38
Sawatch Formation	p. 39
Relationship of Rock Units	p. 41
Chapter 4 Structural Data and Initial Discussion	p. 45
Introduction	p. 45
Faults in the Study Area	p. 45
Fault Descriptions	p. 47
Fault Types and Stereograms	p. 57
Slickenlines	p. 62
Basement Units Separated	p. 64
Basement Structures	p. 68
Cover Structures	p. 70
Basement and Cover Structures	p. 71
Chapter 5 Further Discussion	p. 75
Structural Trend Comparisons	p. 75
Chapter 6 Conclusion	p. 81
Timeline of Deformation	p. 83
Future Research	p. 83
References Cited	p. 85
Appendix	p. 89
Vita	p. 101

LIST OF FIGURES

Figure 1: Satellite image of Colorado with thesis area	p. 2
Figure 2: Topographic map of the thesis field area	p. 4
Figure 3: Red Cliff Bridge over a tributary of the Eagle River	p. 5
Figure 4: Physiographic provinces of Colorado	p. 7
Figure 5: Laramide ranges and uplifts of Colorado	p. 8
Figure 6: Map of Colorado's geology	p. 9
Figure 7: Map of Laurentia with Archean through Neoproterozoic basement features	p. 12
Figure 8: Tectonic map of Proterozoic boundaries in the Southwest U.S.	p. 13
Figure 9: General geology surrounding the Homestake Shear zone area	p. 16
Figure 10: Paleogeographic map of North America during the Late Pennsylvanian from Colorado Plateau Geosystems Inc.	p. 21
Figure 11: Paleogeographic map of North America during the Paleocene around 50 Ma from Colorado Plateau Geosystems Inc.	p. 23
Figure 12: Cross sectional view of the flat slab subduction of the Farallon plate	p. 24
Figure 13: Area of Rio Grande Rifting	p. 25
Figure 14: Cross section of the Rio Grande Rift	p. 26
Figure 15: Outline of the Colorado Mineral Belt and associated mining districts and towns	p. 28
Figure 16: Gilman, Colorado	p. 29
Figure 17: Topographic map of field stops within thesis area	p. 32
Figure 18: Picture of Paleoproterozoic basement	p. 33
Figure 19: Picture of Sawatch Formation	p. 33
Figure 20: Geology of the study area	p. 34
Figure 21: Views of Cross Creek Granite in outcrop	p. 36

Figure 22: Diorite unit in outcrop	p. 37
Figure 23: Views of gneiss in outcrop	p. 38
Figure 24: Biotite crystals in Pegmatite dike	p. 39
Figure 25: View of Sawatch Formation in outcrop	p. 40
Figure 26: Large quartz clast in basal conglomerate	p. 40
Figure 27: Brecciation in Sawatch Formation	p. 41
Figure 28: Felsic dike within Cross Creek Granite	p. 42
Figure 29: Xenoliths of Diorite within Cross Creek Granite	p. 43
Figure 30: Paleo-critical zone and nonconformity	p. 44
Figure 31: Examples of slickenlines	p. 46
Figure 32: Topographic map of localities of fault examples	p. 47
Figure 33: Picture of fault at locality 2	p. 48
Figure 34: Picture of fault at locality 26	p. 49
Figure 35: Picture of fault at locality 27	p. 50
Figure 36: Picture of fault at locality 42	p. 51
Figure 37: Picture of fault at locality 9	p. 52
Figure 38: Picture of fault at locality 10	p. 54
Figure 39: Picture of fault at locality 51	p. 55
Figure 40: Picture of fault at locality 55	p. 56
Figure 41: Stereogram of left-lateral strike-slip faults	p. 58
Figure 42: Stereogram of right-lateral strike slip faults	p. 59
Figure 43: Stereogram of normal faults	p. 60
Figure 44: Stereogram of thrust faults	p. 61
Figure 45: Stereogram of slickenlines	p. 63
Figure 46: Stereogram of diorite planar structures	p. 65
Figure 47: Stereogram of Cross Creek Granite planar structures	p. 66
Figure 48: Stereogram of gneiss planar structures	p. 67
Figure 49: Stereogram of basement planar structures	p. 69
Figure 50: Stereogram of cover planar structures	p. 70

Figure 51: Stereogram of basement and cover planar structures	p. 72
Figure 52: Stereogram of basement and cover faults	p. 76
Figure 53: Stereogram of basement and cover joints	p. 77
Figure 54: Illustration of tectonic and geologic events	p. 80

LIST OF TABLES

- Table 1: Summary of fault data from stereograms in figures 41-44 p. 62
- Table 2: Summary of basement unit data from stereograms in
figures 46-48 p. 68
- Table 3: Summary of fault data from stereograms in figures 49-50 p. 71

CHAPTER 1

Introduction

In the northeast Sawatch Mountains of central Colorado, the late Cambrian Sawatch Formation nonconformably overlies Paleoproterozoic basement rocks that include granite, diorite and gneiss. These rocks are highly jointed, faulted and locally mylonitized, while the overlying Sawatch rocks have only joints and faults. This study is a detailed examination of the nature and orientation of structures in the basement and cover rocks in the study area. This has made it possible to determine which structures are unique to, and which are shared between, basement and cover rocks. This has allowed speculation about which structures in the Sawatch Formation may have inherited their trend from structural patterns in the underlying basement rocks and the timing of deformation in the area.

In this study, the structural relationships between basement rocks and the overlying Sawatch Formation were researched. Brittle features in the basement and cover rocks were examined to determine structural relationships between the units. This allowed the determination of a geologic history for the development of structures over time. The orientations of joints, faults and sense-of-shear indicators such as slickenlines, within the basement and cover units

were measured during field work. An interpretation of the structural history of the study area has been delineated by determining which structures are common to both Proterozoic and Paleozoic rocks and which structures are found only in one or the other.

The Sawatch Range is a Laramide age, basement-cored anticline that has numerous mountains that exceed 14,000 feet in elevation, including the highest peak in Colorado, Mount Elbert (14,439 feet). The thesis area is located on the northeast flank of the Sawatch anticline in central Colorado (Fig. 1). On the



Figure 1. Satellite image of Colorado with the thesis field area marked by a gold star (modified from Google Maps, 2017).

northeast flank of the northern part of the Sawatch Range, a nonconformity between uplifted crystalline basement rocks and overlying Paleozoic cover rocks is exposed.

North of Leadville, Colorado, U.S. Highway 24 follows the flank of the Sawatch anticline and passes abandoned mines and the ghost town of Gilman and the small town of Red Cliff. Both were founded as mining centers during the silver and gold booms of the 1880's. The field area is located along U.S. Highway 24 and the Eagle River, northwest of Red Cliff in Eagle County, Colorado (Figures 2 and 3) in the Minturn Quadrangle. Previous scientific research in this area includes studies by Ogden Tweto and T.S. Lovering, who conducted mapping and geologic investigations of this region for the U.S. Geological Survey from the 1940's to the 1980's. The Colorado Geological Survey also mapped the area in 2012 (Kirkham et. al, 2012). These earlier studies established the broad geologic framework of the area but did not focus on details of the structural relationships between the basement rocks and the overlying cover strata.

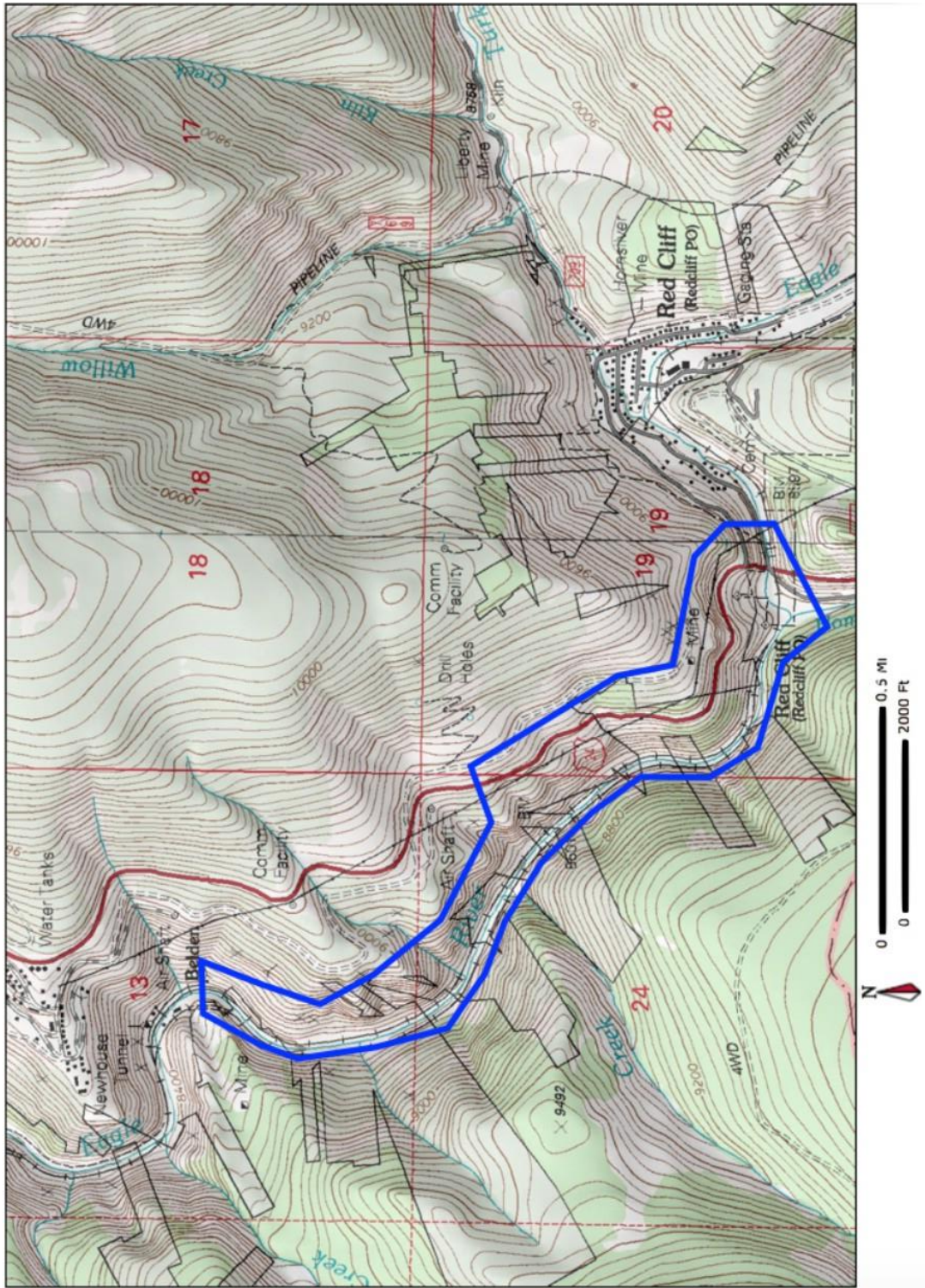


Figure 2. Topographic map of the thesis field area outlined in blue with surrounding towns (modified from MyTopo.com, 2017).



Figure 3. *Red Cliff Bridge over the Eagle River (to the right on the image). The Sawatch Formation makes a prominent cliff above US Highway 24 in the left part of the image. Basement rocks are exposed on the hill on the far side of the bridge with a part of the Sawatch Formation on top of the hill. View is to the south.*

CHAPTER 2

Geologic Setting and Previous Works

Regional Geology and Structure

Colorado has had a complex geologic history with multiple orogenic influences. The result is an area of mountainous uplifts that expose deep crystalline basement rocks that are buried elsewhere.

Colorado's distinctive and varied topography reflects geologic events and processes that make the state an excellent outdoor geologic laboratory. The physiographic provinces of Colorado can be separated into five areas of different overall geologic features (Matthews et al., 2009). These include the Middle Rocky Mountains, Colorado Plateau, Southern Rocky Mountains, Colorado Piedmont and Great Plains (Matthews et al., 2009; Fig. 4). The mountains present in Colorado today are mainly the product of Laramide uplifting (which began in the late Cretaceous) and Quaternary Ice Age glaciation. Basins created during the Laramide orogeny captured sediments from the uplifted mountains and provide a record of events during uplifting (Tweto, 1980).

In the southern Rocky Mountains province, ridges and uplifts created during the Laramide orogeny include the Uncompahgre-San Luis Highland and the Sawatch Range ~ 70 Ma (Tweto, 1980). This was followed by uplifting of the

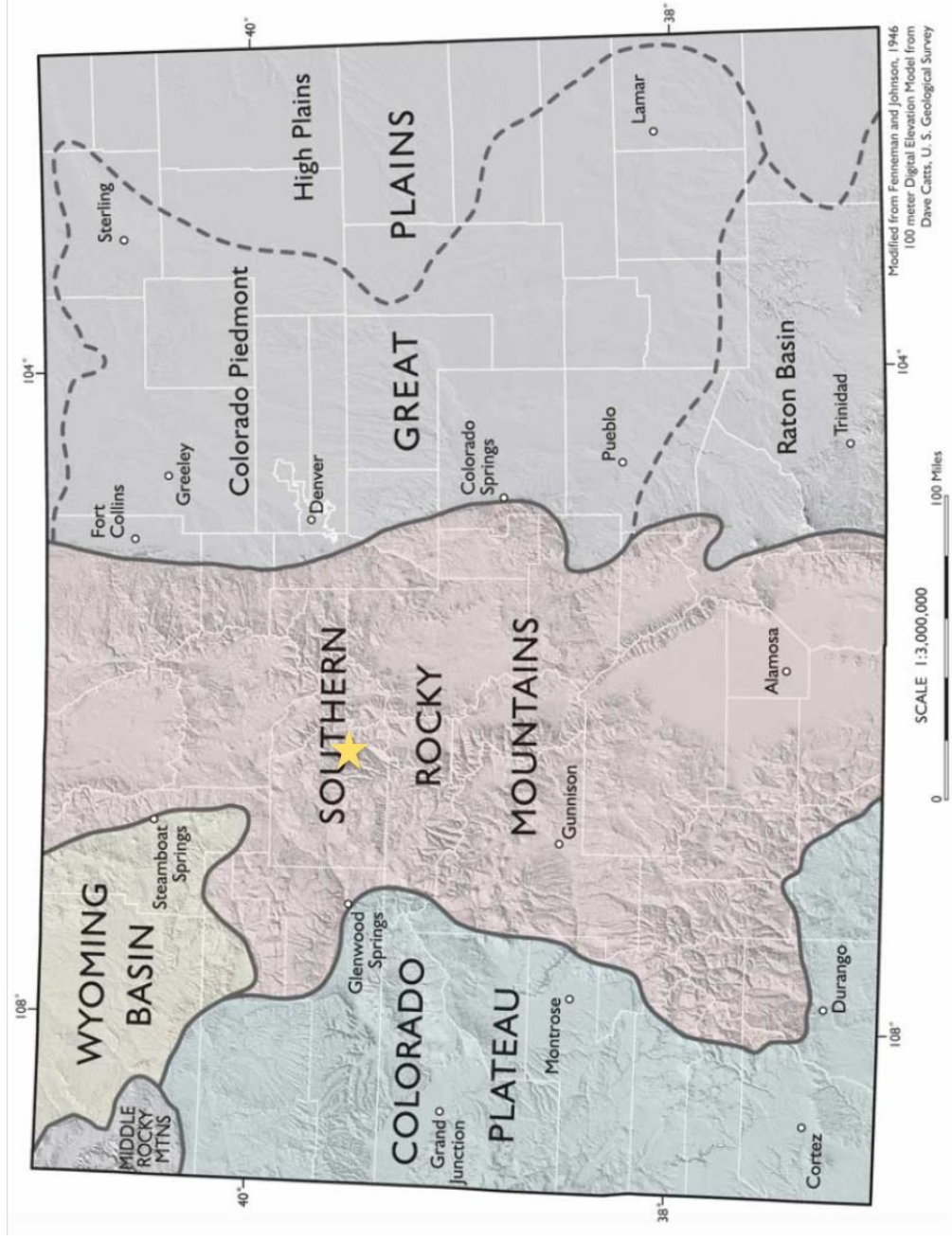


Figure 4. Physiographic provinces of Colorado. The thesis area is marked with the gold star. (modified from Colorado Geological Survey, 2016).

Gore, Front, Park Ranges and the Uinta and Needle mountains 70 to 65 Ma (Tweto, 1980, Fig. 5). Most of these uplifts are anticlines cored by igneous and

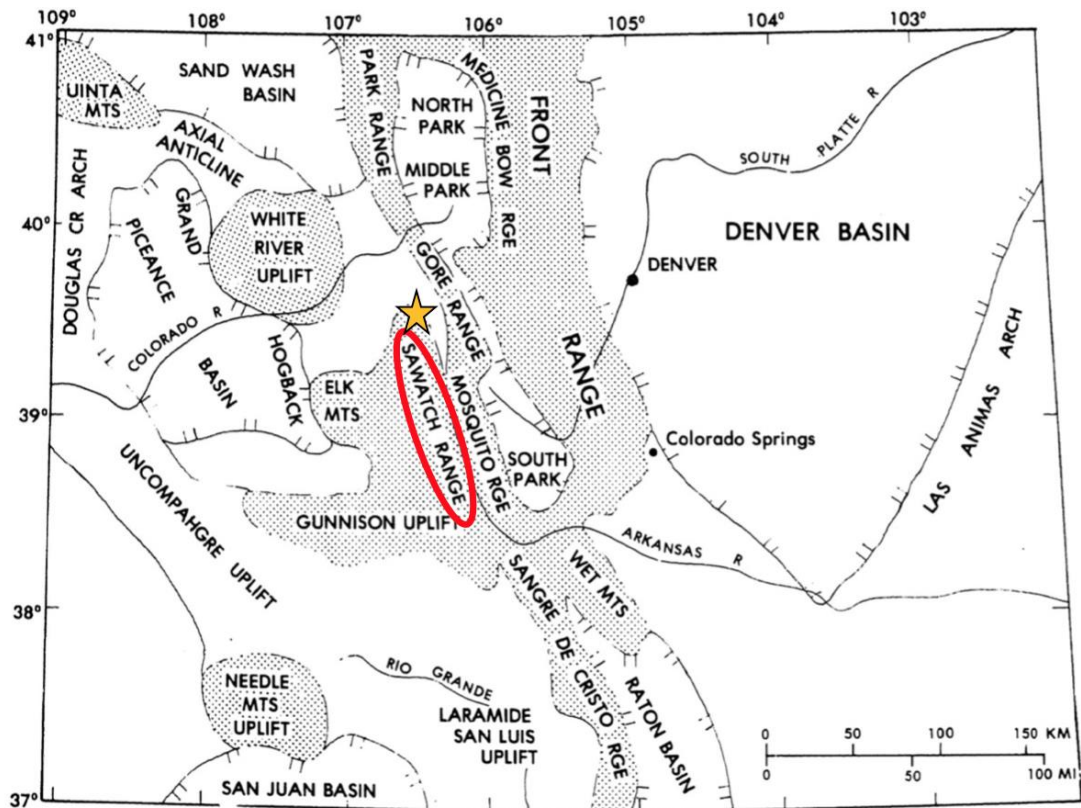


Figure 5. Laramide ranges and uplifts of Colorado. Note the Sawatch Range in central Colorado (modified from Tweto, 1980).

metamorphic rocks. A simplified geologic map of Colorado is shown in Figure 6.

The Sawatch Mountains are a northwest-southeast trending range that extend for about 85 miles as a part of the Rocky Mountains of central Colorado. The Sawatch Range formed as an anticline about 70 Ma, at the beginning of the Laramide orogeny (Reed, 2009). The Mosquito Range is on the east flank of the

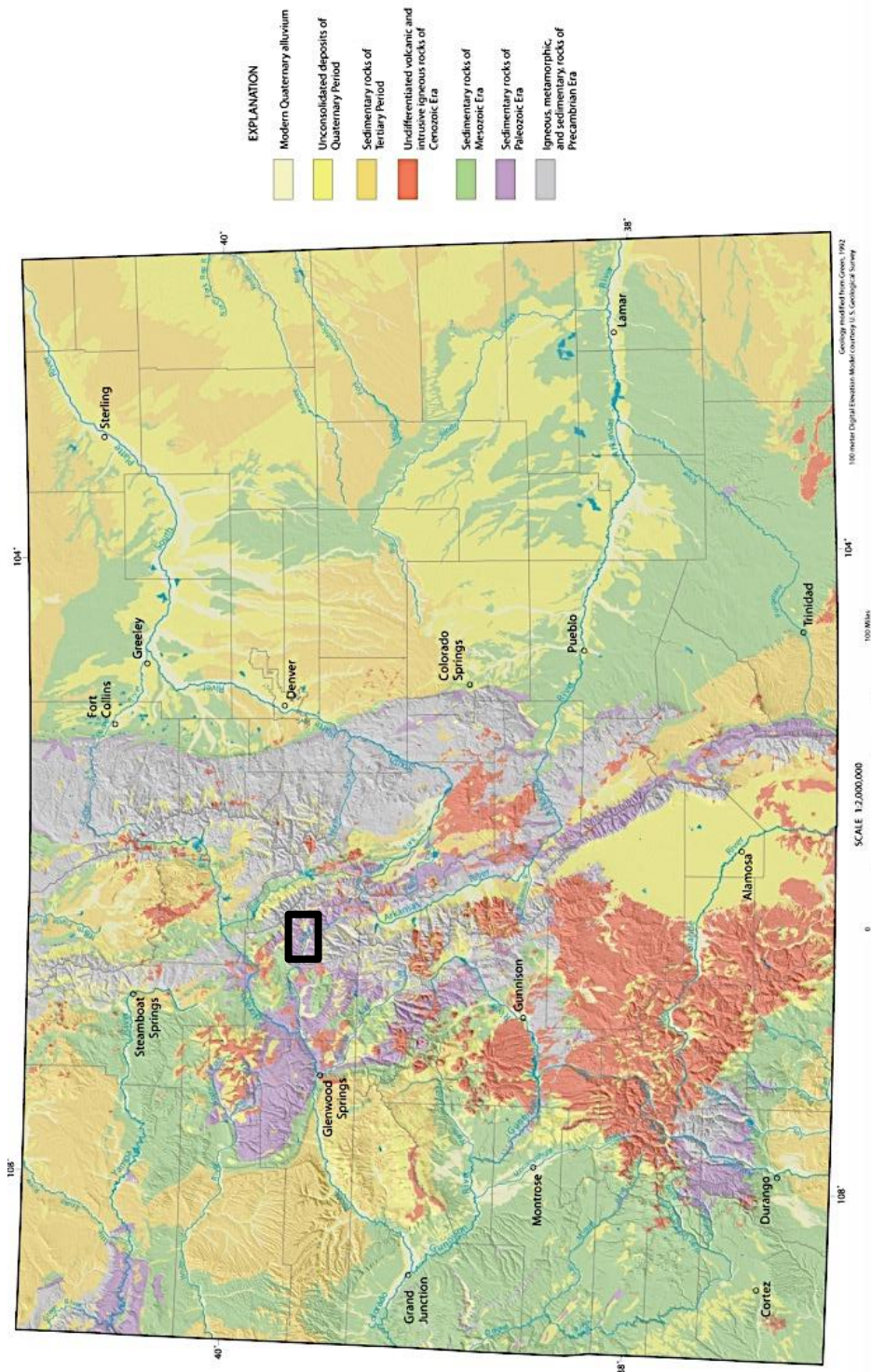


Figure 6. Map of Colorado's geology. The study area is marked with the black square. The map shows mainly Precambrian and Paleozoic units in the thesis area and in the Rocky Mountains (modified from Colorado Geological Survey, 2016).

anticline and the west flank is the Elk Mountains (Fig. 5); both are thrust, folded and intruded by Oligocene igneous rocks (Tweto, 1975).

The late Cambrian Sawatch Formation nonconformably overlies Paleoproterozoic basement rock (Allen, 2004), and the relationship between those two units is central to this study. Cambrian and Mississippian strata that are uplifted in the Sawatch Range have been interpreted as shallow shelf and peritidal facies (Allen, 2004). Within the Paleozoic age strata in this area, there are five unconformities indicating transgressive cycles, regressive cycles and local uplifts (Allen, 2004).

Tectonic Evolution and Stratigraphy of the Central Rocky Mountains

Precambrian Geology of Southwest Laurentia

Introduction: Island Arc Accretion

The basement rocks of North America provide insight into the plate tectonic history of Laurentia, the ancient landmass that developed into North America. Laurentia initially formed by a series of accretions during the Paleoproterozoic, about 2.0 to 1.8 Ga. The initial continental accretions consisted of Archean crustal material of continents and fragments of continents (Whitmeyer et al., 2007). These accretions of Archean crust were a part of the Trans-Hudson orogeny that was similar to the Himalayan orogeny of today (Whitmeyer et al., 2007). Additional volcanic island arcs and slivers of continental crust accreted onto the Archean crust from 1.8 to 1.0 Ga and is what constitutes most of the basement rock for North America and the United States (Whitmeyer et al., 2007, Fig. 7).

Proterozoic rocks span the state of Colorado and are the basement rock for the state. In Colorado and farther south, several linear crustal provinces were accreted to Laurentia during the Paleoproterozoic between 2.0 Ga to 1.8 Ga (Jones et al., 2009, Fig. 8). These accretionary provinces consisted of multiple

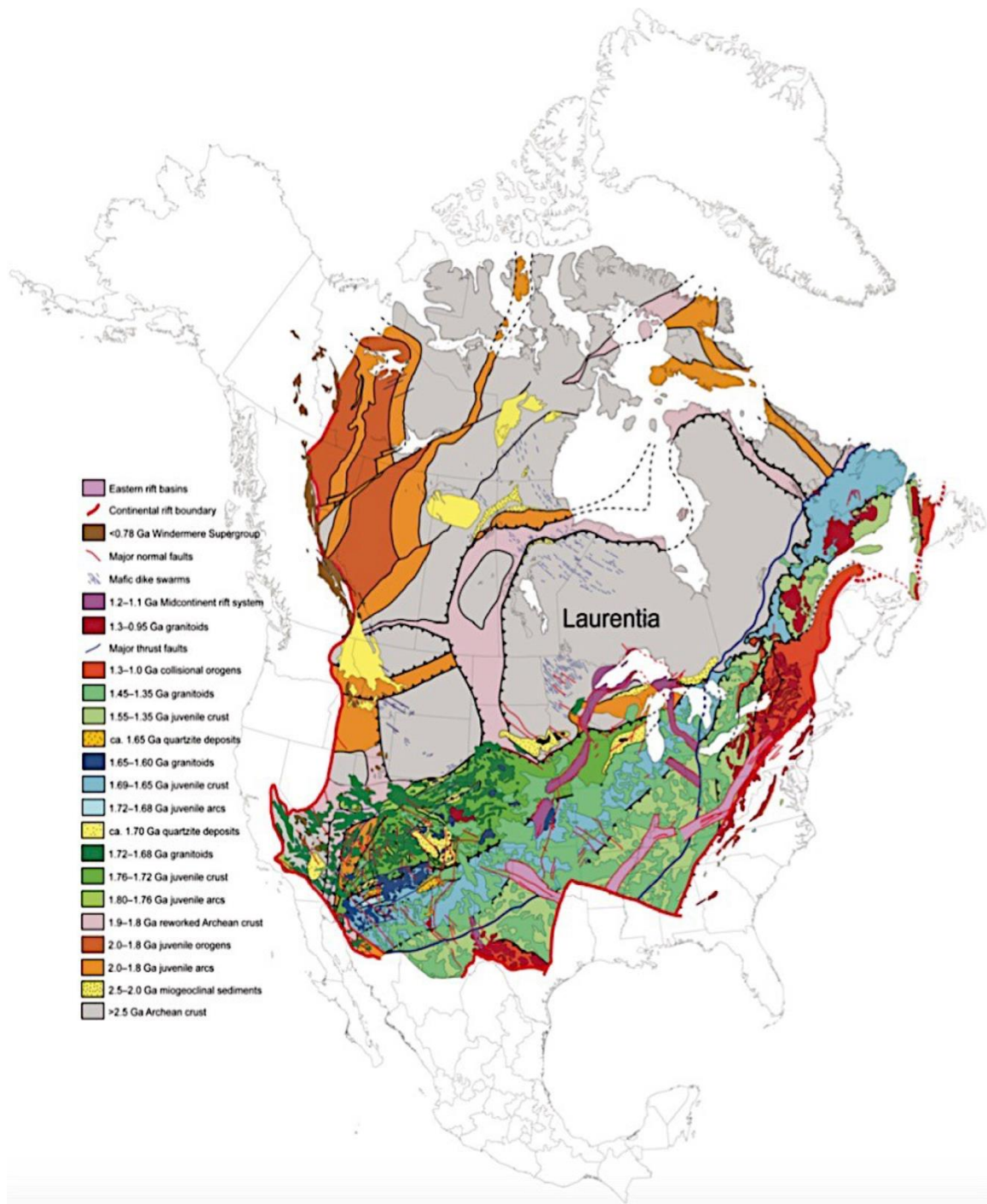


Figure 7. Map of Laurentia with Archean through Neoproterozoic basement features (from Whitmeyer et al., 2007).

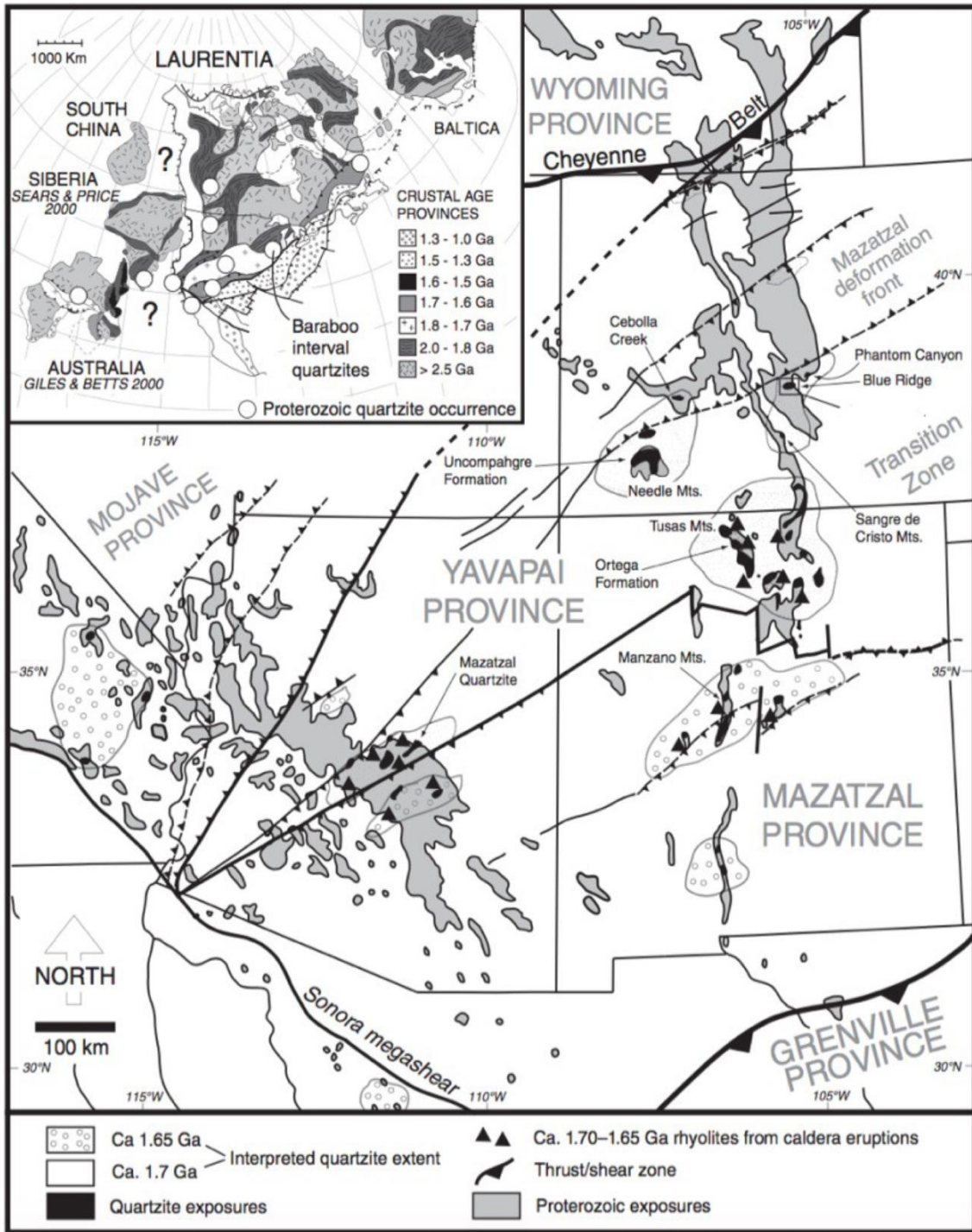


Figure 8. Tectonic map of Proterozoic boundaries in the Southwest U.S. (from Jones et al., 2009).

blocks separated by shear zones that formed the Mojave, Yavapai and Mazatzal provinces (Whitmeyer et al., 2007; Fig. 8). The Yavapai and Mazatzal belts are discussed in more detail below. Continued growth of Laurentia to the south occurred with the Grenville orogeny (1.2 Ga) and the assembly of the supercontinent Rodinia (Jones et al., 2009). The breakup of Rodinia occurred during the Neoproterozoic (Chapin et al., 2014).

Yavapai Province

The Yavapai province trends to the northeast and southwest across parts of several central and southwestern states: primarily Nebraska, Colorado and Arizona (Fig. 8). The province represents an accumulation of juvenile arc terranes (Jones et al., 2009). The Yavapai orogeny was a progressive orogenic event that peaked at ~ 1.71 to 1.68 Ga and accreted arc terranes with the rest of Laurentia (Whitmeyer et al., 2007; Jones et al., 2009).

Mazatzal Province

The southern margin of Laurentia experienced shortening and then the accretion of the Mazatzal province during the 1.66 Ga to 1.60 Ga Mazatzal orogeny (Lee et al., 2012). The Mazatzal province is south of the Yavapai

province and is located in Arizona and New Mexico (Jones et al., 2009). The province consists of sedimentary and juvenile arc related igneous rocks that were deformed during the Mazatzal orogeny (Amato et al., 2008). The suture zone between the Yavapai and Mazatzal provinces is thought to be located along the Jemez lineament in New Mexico, and is interpreted to be an interwedging of crustal blocks of a bivergent orogen (Whitmeyer et al., 2007). The orogeny was followed by a period of continental stability for about 200 Ma until reactivation and magmatism around 1.4 Ga (Lee et al., 2012). At this time, the St. Kevin batholith formed along the southwest portion of the Homestake shear zone (Allen et al., 2013).

Precambrian Shear Zones of Colorado

Shear zones, faults and folds formed during the remainder of the Precambrian. The deformational histories of Precambrian rocks are complex due to the many events they have experienced and the structures in the rocks are therefore complex as well. The Homestake shear zone (HSZ) is a northeast trending lineament that is exposed in the Sawatch Range of the Colorado Rockies and is located in the northern section of the Colorado Mineral Belt (a feature described in more detail later; Fig. 9). The HSZ consists of multiple individual shear zones and has an aggregate width of

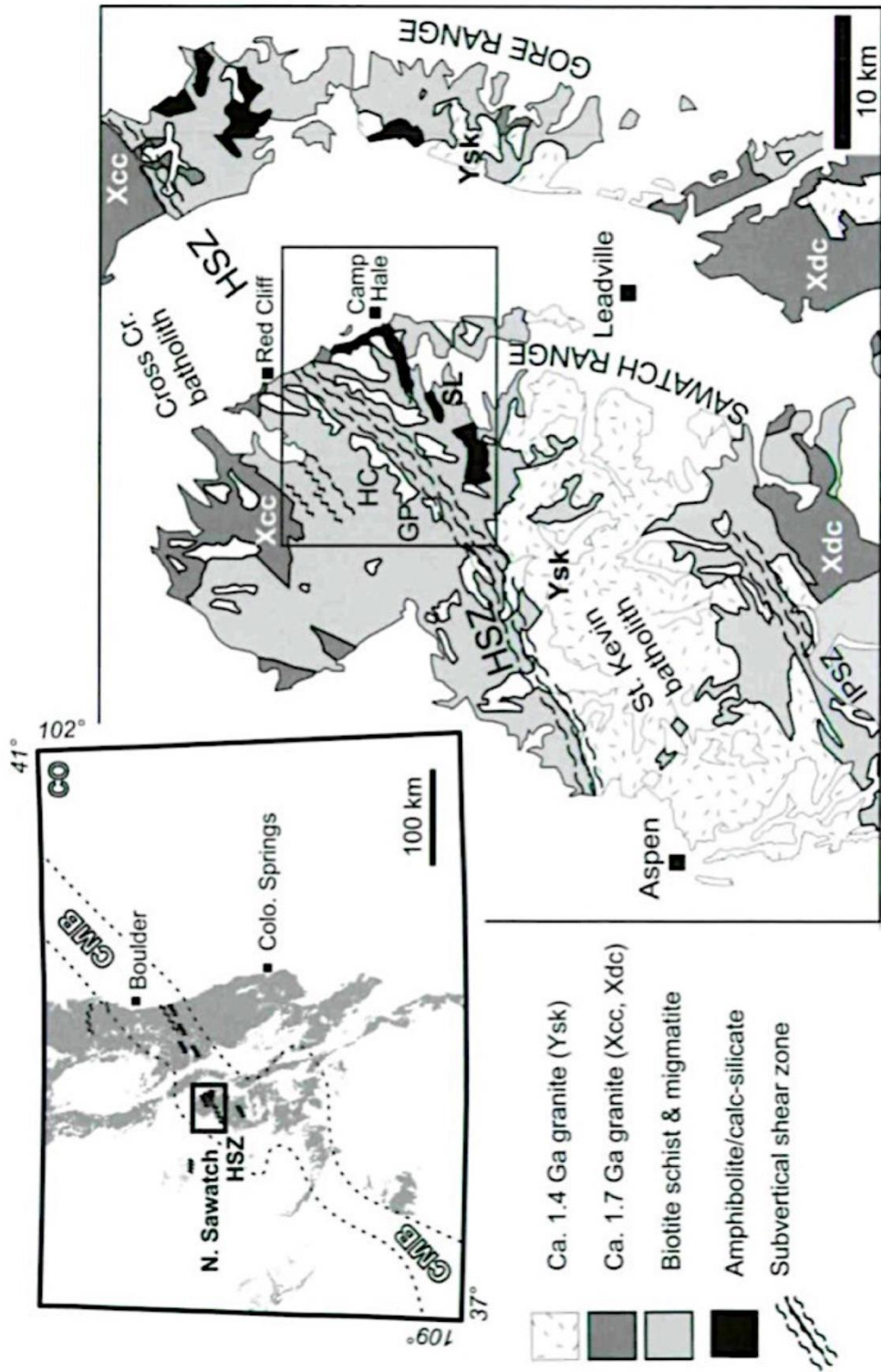


Figure 9. General geology surrounding the Homestake shear zone area, showing granites, metamorphic units and subvertical shear zones and the Colorado Mineral Belt outlined in the dotted line (from Shaw et al., 2007).

6.2 miles (10km) (Tweto, 1977). The HSZ passes a few miles south of the study area. The HSZ consists mainly of Mesoproterozoic mylonites that deformed 1.8-1.6 Ga high temperature, migmatitic schist and gneiss (Lee et al., 2012). The country rock around the shear zone is described as a locally migmatitic biotite gneiss and schist, calc-silicate gneiss, mafic to ultramafic pods and alkaline mafic dikes (Lee et al., 2012). The HSZ may have formed as a wide zone of plastic flow and folding and as time progressed evolved into a series of narrower parallel shear zones and fault systems (Shaw et al., 2007).

Paleoproterozoic Rocks in the Study Area: Cross Creek Granite, Diorite and Gneiss

There are three main units forming the Proterozoic basement rocks in the study area: The Cross Creek Granite, a diorite unit and a gneiss unit. The Cross Creek Granite is Paleoproterozoic in age and dated to be about 1.71 Ga (Kirkham et al., 2011). It has been described as heterogeneous gray to pink in color, fine- to coarse-grained, with areas being foliated- to non-foliated; the amount of foliations within the unit varies throughout the area (Kirkham et al., 2011; Tweto et al., 1977). The appearance and composition of the granite is commonly variable because the distribution of potassium feldspar within the unit is irregular (Tweto et al., 1977). The granite is thought to be associated with a

batholith emplacement (Tweto et al., 1977). The granite contains xenoliths of gneiss and migmatites (Tweto et al., 1977). The Cross Creek Granite is thought to be synorogenic with the Yavapai orogeny and related to the Routt Plutonic Suite at 1.7 Ga (Kirkham et al., 2011). The Cross Creek Granite batholith possibly intruded into the biotite gneisses as the batholith was rising up through the crust (Tweto et al., 1977).

The diorite unit in this area is described as dark gray, fine to medium grained, foliated to non-foliated with dominantly biotite and amphibole (Kirkham et al., 2011). Inclusions of the diorite are found within the Cross Creek Granite and it is thought to represent an early crystalline phase of the Cross Creek Granite (Kirkham et al., 2011).

The gneiss unit has been described as containing biotite, quartz and plagioclase (Tweto et al., 1977). The gneiss is thought to be the oldest unit in the area based on rubidium-strontium dating and metamorphism of this unit was determined to be at 1.7 to 1.8 Ga (Tweto et al., 1977). The gneiss exhibits sub-vertical foliation defined by biotite, quartz and plagioclase (Allen et al., 2002). Mylonitic gneisses in the area could have been formed from ductile shearing of metasedimentary basement rocks along strands of the Homestake shear zone or deformed at the same time as the intrusion of the Cross Creek Granite (Kirkham et al., 2011).

Paleozoic Geology

Paleozoic Rocks in the Study Area: Cambrian Sawatch Sandstone

The Sawatch Formation is found in various locations across the state of Colorado and it is the oldest Paleozoic formation along the Front Range (Brainerd, et al., 1933). The formation was named by G. H. Eldridge who observed it within the Sawatch Range (Brainerd, et al., 1933).

The Cambrian Sawatch Formation sandstone rests nonconformably on the Paleoproterozoic basement strata in the study area. In the study area, the paleocritical zone between the Paleoproterozoic basement rocks and the base of the Sawatch Formation is highly weathered and friable. The paleocritical zone does not exhibit evidence of paleosols, and represents an erosional surface.

The Sawatch Formation has been described as a white to light pinkish quartz sandstone with silica cement that is well indurated (Kirkham et al., 2011). The formation contains some hematite, feldspar and glauconite (Kirkham et al., 2011). The Sawatch Formation is fine-grained, is about 200 feet thick and contains a basal conglomerate (Kirkham et al., 2011). Quartz granules of the basal conglomerate are sub-rounded to sub-angular and about 3-6 mm in diameter. (Tweto et al., 1977).

The Sawatch Formation can be separated into lower, middle and upper informal members (Myrow et al., 2003). The lower member consists of sandstone

and conglomeratic sandstone; the middle member consists of interbedded sandstone, dolomitic sandstone and mudstone and the upper member is sandstone (Allen, 2004). The paleoenvironment of the upper and lower members in the Sawatch Formation is thought to have been deposited in a shallow marine environment (Myrow et al., 2003). The middle member represents a subaqueous, tidally influenced environment deposited during a transgressive sequence (Myrow et al., 2003).

Ancestral Rocky Mountains

The Ancestral Rockies were uplifted intracratonic blocks and en-echelon folds that formed during the middle Pennsylvanian (Chapin et al., 2014; Kluth, 1986). The processes that caused the uplift are debated. A hypothesis for the uplift is far field stresses associated with the Ouachita orogeny that were generated by the collision of Laurentia with Gondwana (Chapin et al., 2014; Kluth, 1986). These collisions were a part of the creation of the supercontinent Pangea. The Ancestral Rockies covered an area of about 2,000 kilometers northwest from Llano, Texas to southern Idaho (Chapin et al., 2014, Figure 10), but were mainly in New Mexico and Colorado.



Figure 10. *Paleogeographic map of North America during the Late Pennsylvanian, the Colorado border is in red, major Ancestral Rocky Mountain uplifts are outlined in purple. (modified from Colorado Plateau Geosystems Inc.)*

As the Ouachita orogeny progressed, deformation moved farther into the foreland. Because the collisional zone shifted southwestward throughout the Pennsylvanian, uplift of the Ancestral Rockies shifted to the northwest in an intraplate response to the orogeny (Kluth, 1986). During the Triassic and

Jurassic, Pangea rifted apart to form today's continents. By the mid Jurassic, the Ancestral Rockies were highly eroded and were covered by alluvial and lacustrine deposits before the generation of the Western Interior Seaway (Kellogg et al., 2004).

Mesozoic Geology and the Laramide Orogeny

Another major tectonic event to affect Colorado and the western United States was the late Cretaceous to Paleogene Laramide orogeny (Weil et al., 2016, Fig. 11). Laramide deformation occurred from 75 to 50 Ma (Weil et al., 2016). The Sawatch Range is a Laramide orogenic basement cored uplift. Uplifted areas associated with the Laramide orogeny are thick-skin basement cored ranges with a northwest-southeast to north-south structural trend and are separated by basins (Weil et al., 2016). Flat slab subduction of the Farallon plate oriented to the northeast-southwest caused the uplift (Weil et al., 2016).

With the flat slab subduction of the Farallon plate, instead of the plate descending downward at the subduction zone (as is the usual case), it maintained a flat angle beneath the continental crust and possibly did not start to descend until it was far inland of the continental edge (Nesse, 2006, Fig. 12). The amount of Laramide uplift is estimated to have been around 4.5 to 5 km, but erosion that removed material from the top of ranges has made this uncertain (Nesse, 2006).



Figure 11. Paleogeographic map of North America during the Paleocene around 50 Ma, the Colorado border is in red. (modified from Colorado Plateau Geosystems Inc.).

Uplifts and basins in Colorado created during the Laramide orogeny are shown in Figure 5. The first areas to be uplifted during the Laramide were the Uncompahgre-San Luis highland and the Sawatch Range around 70 Ma (Tweto, 1980). This was followed by the uplifting of the Gore, Front and Park ranges and the Uinta and Needle mountains at ~ 70 to 65 Ma (Tweto, 1980).

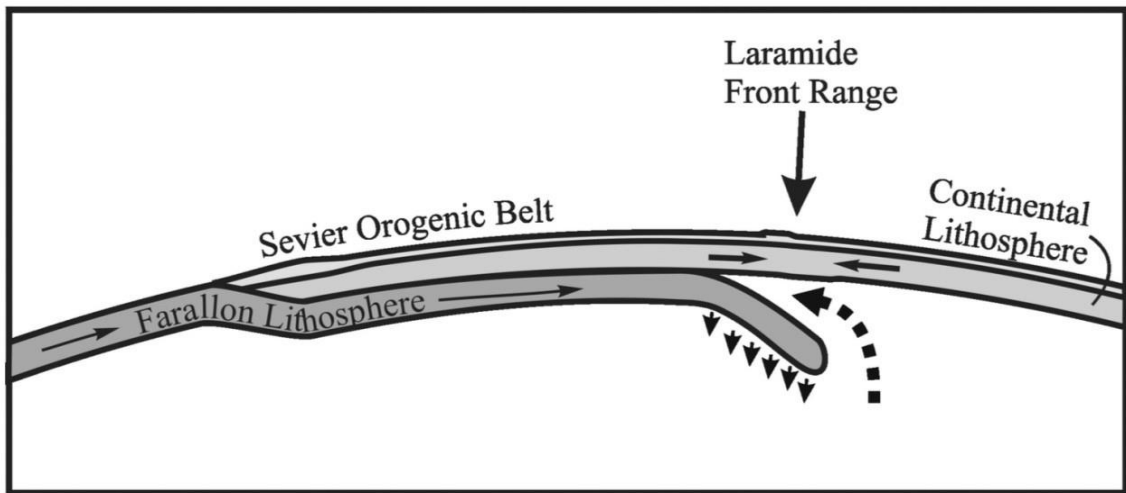


Figure 12. Cross sectional view of the flat slab subduction of the Farallon plate (from Nesse, 2006).

Cenozoic Geology: Igneous Activity and Rio Grande Rifting

Widespread igneous activity in Colorado began at ~ 36 Ma and continued for about 10 million years (Matthews et al., 2009). Volcanic ash flows and mudflows deposited over low relief post-Laramide erosional surfaces and the extent of volcanic deposition covered half of Colorado (Matthews et al., 2009).

The Rio Grande rift may have influenced the geology of the study area, as it is proximal to the study area. The rift spans a distance of about 324 miles (550km) south from west Texas, north to Leadville, Colorado (Chapin et al., 1994, Fig. 13). It is a en-echelon belt of north striking basins that formed around 36 to 37 million years ago (Kelly et al., 2012). The basins of the Rio Grande Rift

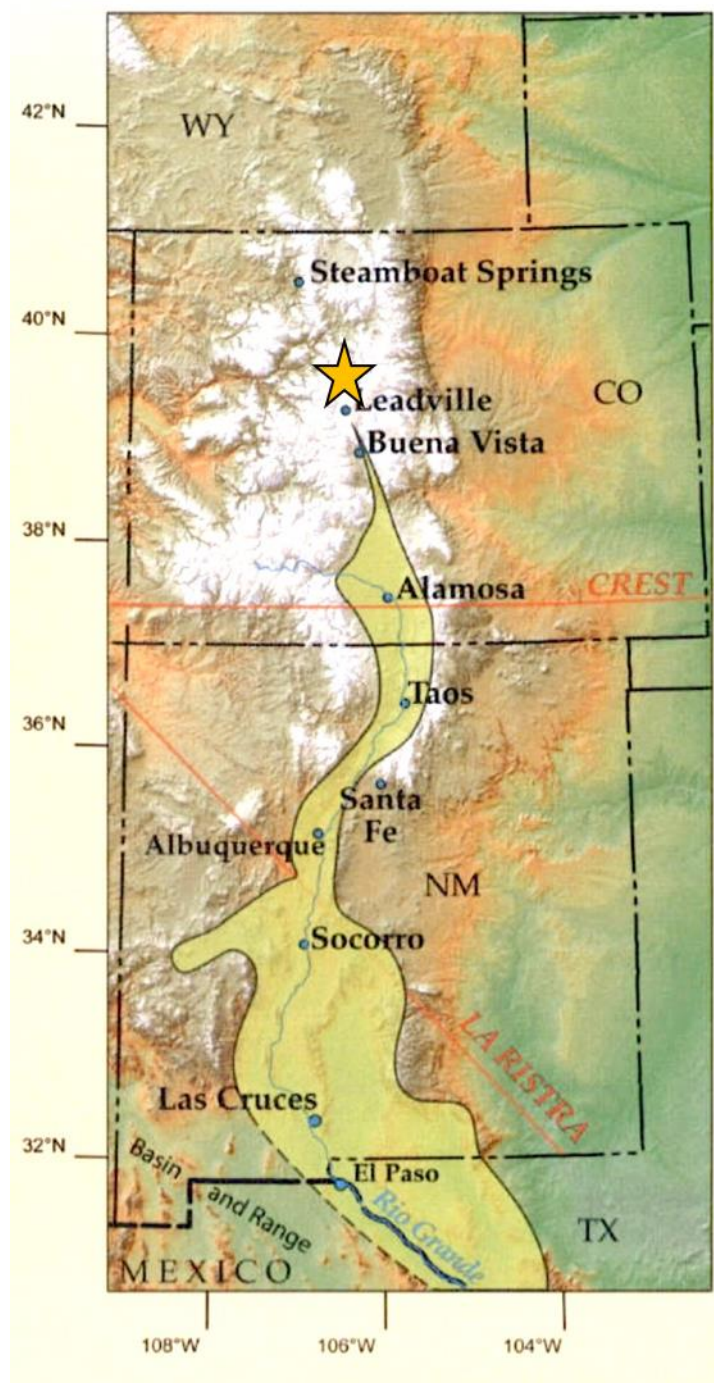


Figure 13. Area of Rio Grande rifting shown in yellow and the study area marked with a gold star (modified from Kelly et al., 2012).

can be separated into four main parts: the Albuquerque, Española, San Luis and the Upper Arkansas basins (Chapin et al., 1994). The onset of Rio Grande rifting included pyroclastic volcanism located near and within the rift basins (Chapin et al., 1994). Asymmetric half grabens (Fig. 14) comprise the overall

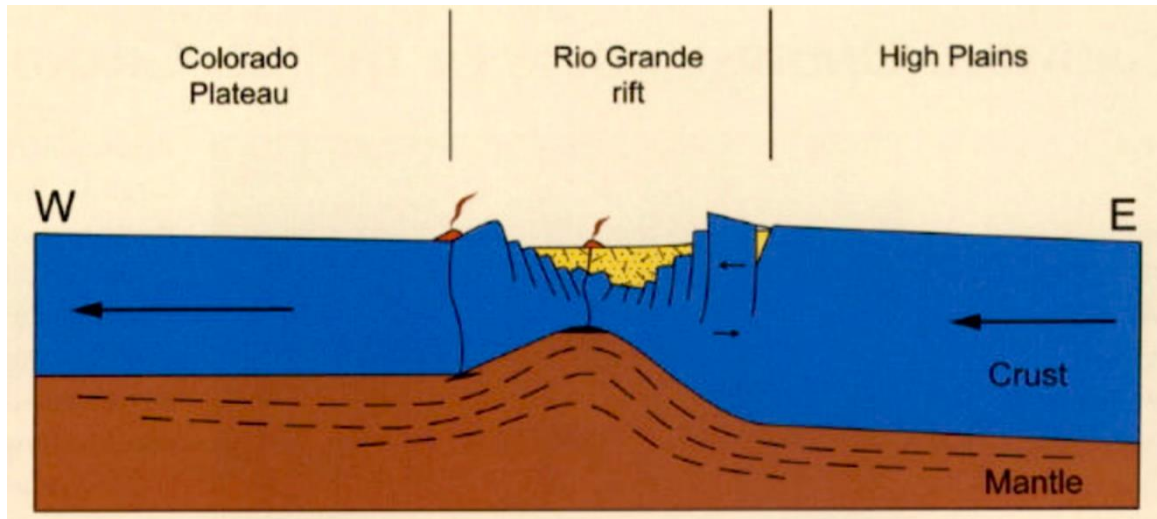


Figure 14. Cross section of the Rio Grande Rift (from Kelly et al., 2012).

geometry of the rift (Chapin et al., 1994).

The eastern and western sections of the rift are not symmetrical in geometry and have different geological features. The eastern margin has prominent hot spots, volcanics and is higher in elevation than the western margin (Kelly et al., 2012). The higher elevation in the east could be due to continental crust moving up on a bulge of mantle (Kelly et al., 2012; Fig. 13). It is suggested from this evidence that continental crust to the west of the rift is moving at a faster rate than continental crust on the eastern side (Kelly et al., 2012). The rifting creates crustal thinning and upwelling of the mantle beneath the thinned crust, which is located along the western margin (Kelly et al., 2012).

Colorado Mineral Belt

The Colorado Mineral Belt (CMB) (Figure 15) is a northeast-southwest striking belt of mineralization across Colorado. The CMB is ~15 to 30 miles (25-50km) wide and about 310 miles (500km) long ranging from the La Plata mountains in southern Colorado to the Front Range of Boulder Colorado (Chapin et al., 2012; Curtis, 1997). It trends northeast-southwest, contrary to the trend of most ranges in Colorado, including the Sawatch Range.

The belt is mainly composed of alkaline granodiorites in the central portion and quartz monzonite stocks in the northeast, often containing base metal deposits of lead, zinc and copper and rarer precious metal deposits of gold, silver and molybdenum (Chapin et al., 2012, Matthews et al., 2009). Over 400 mineral species have been found in the Colorado Mineral Belt, 42 of which were previously unknown (Curtis, 1997). The emplacement of economic minerals and ore bodies is associated with igneous plutons and veins created during the Laramide orogeny from the late Cretaceous to the Eocene about 72 to 36 Ma (Curtis, 1997).

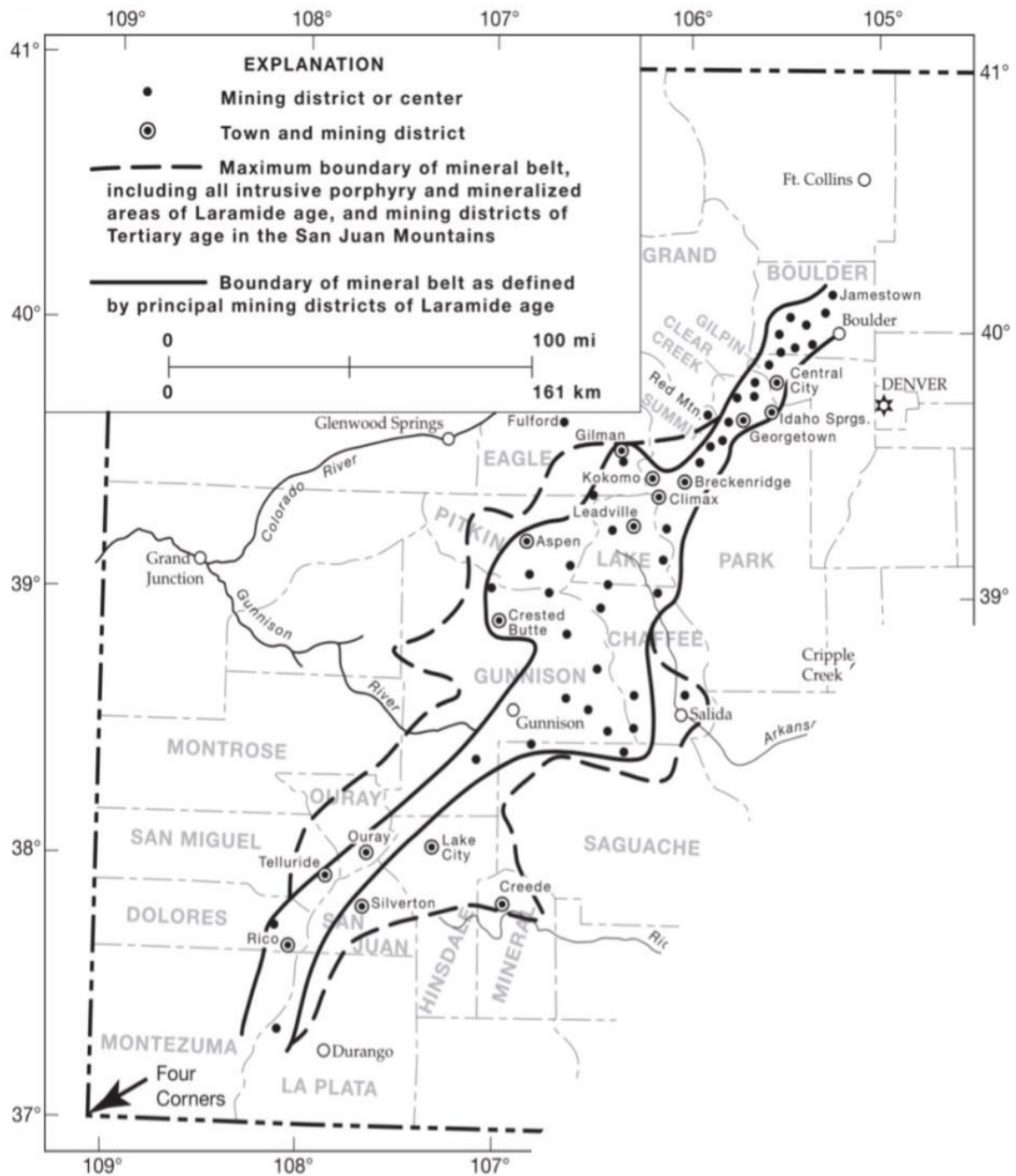


Figure 15. Outline of the Colorado Mineral Belt and associated mining districts and towns (modified from Chapin et al., 2012).

Mining History

The ghost town of Gilman, Colorado is located along U.S. Highway 24, about 6 miles south of Minturn, and about 4 miles north of Red Cliff, Colorado (Fig. 16). The large abandoned Eagle mine at Gilman is immediately north of the



Figure 16. *Gilman, Colorado. Picture taken viewing to the North.*

study area. Gilman is located on the northwestern edge of the Colorado Mineral Belt (Lovering et al., 1978). Access to the mine is restricted due to environmental concerns and therefore the mine area cannot be included in this study.

The mining company town was founded in the 1880's just after silver and

gold strikes in Leadville, Colorado, from 1877 to 1878 (Murphy, 2002). In 1881, the *Denver and Rio Grande* narrow gauge railroad was constructed from Leadville to the mining area along the Eagle River. Ores were transferred from the older mine operations on the canyon cliffs by aerial or rail trams down to the railroad (Lovering et al., 1978). In the area's early history, numerous small mines were built along the Eagle River canyon until the Eagle mine was built at the present location in 1918 by the New Jersey Zinc Company after which mining operations along the Eagle River were carried out primarily in that location (Lovering et al., 1978). The source of the ore solution is believed to be from a magma body (Lovering et al., 1978). The Eagle mine closed in 1984 and after closing, the EPA initiated cleanup and remediation of the area.

CHAPTER 3

Methods and Field Observations

Introduction

This research focused on analysis of geologic structures in the basement rocks and in the nonconformably overlying Sawatch Formation in the area between Red Cliff and Gilman, Colorado (Figures 2, 17). The research area includes Paleoproterozoic basement outcrops (Fig. 18) along 1.5 miles of the Eagle River and Sawatch Formation outcrops (Fig. 19) adjacent to U.S. Highway 24 at an average elevation of 9,000 feet. Field work was conducted in the summer of 2016 over the course of three weeks in July and August.

The field area is located four miles north of the Homestake Shear zone (Fig. 9) and is just south of the Eagle Mine Superfund site. Earlier regional geologic maps by T.S. Lovering and Ogden Tweto (1940-41, 1946, 1961) and the Colorado Geological Survey in 2012 (Fig. 20) were used as references for the study area.

Structural features of the basement and cover units that were measured include joints, faults, folds, sense-of-shear indicators, bedding planes, foliation planes, lineations and slickenlines. Strike and dip and trend and plunge of these

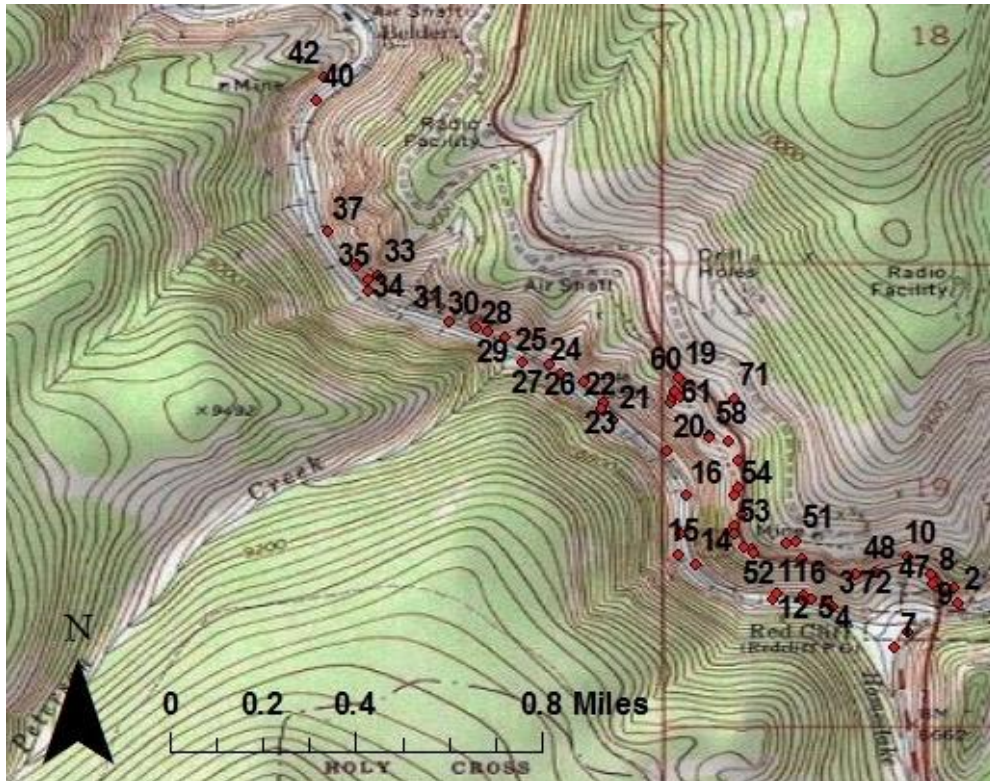


Figure 17. *Topographic map of localities of field stops within the thesis area. These locations are given in the appendix.*

features were measured. A total of 283 structural features were measured. GPS locations were taken where structural data was collected, photographs were taken of geologic structures and descriptions and interpretations of the structures were made.

Data analysis was used to help determine the orientation and characteristics of the structural features within the basement and cover units. Software used for analysis of the data included applications from Midland Valley (Field Move Clino) and Stereonet 9 by Richard W. Allmendinger. The Field Move Clino iPhone application was used in addition to field notebooks to aid with data



Figure 18. *Paleoproterozoic basement rocks along the abandoned Denver and Rio Grande railroad tracks as viewed to the north. The Eagle River is about 15 feet to the left of the railroad tracks.*



Figure 19. *Sawatch Formation viewed to the north on the right, forming a cliff above U.S. Highway 24. Eagle River Gorge runs along the west (left) side of the highway.*

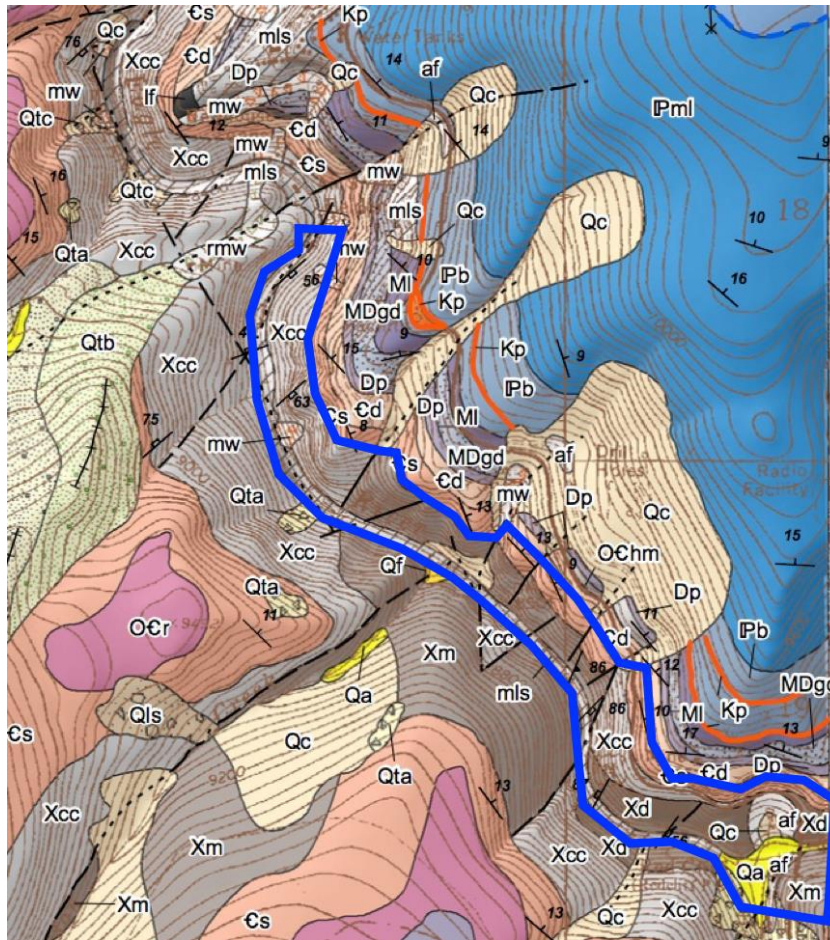


Figure 20. Geology of the study area (outlined in blue). Relevant units include: diorite (Xd), Cross Creek Granite (Xcc), migmatite, biotite and schist (Xm) and Sawatch Sandstone (ϵ_s) (Modified from Kirkham et al. 2012).

collection and analysis in the field and was used to take images with GPS coordinates and note taking in the field. Stereograms were created with Stereonet 9 and were plotted as equal area projections to determine structural trends.

Description of Rock Units

Introduction

The units of the Paleoproterozoic basement rocks of the thesis area include the Cross Creek Granite, diorite and gneiss, which are nonconformably overlain by the late Cambrian Sawatch Formation sandstone. The units are cliff formers along the Eagle River gorge and are stained black in many areas along the river canyon in part due to the smoke from the trains that previously ran along the *Denver Rio Grande* railroad. Field descriptions of the units are provided below.

Cross Creek Granite

The Cross Creek Granite (Fig. 21) in the thesis area is heterogeneous in character. The granite within the study area on fresh surfaces is dark gray with large orthoclase crystals in some areas and in other areas is pink in color. The granite ranges from porphyritic to phaneritic in texture and contains potassium feldspar, quartz, sodium plagioclase, biotite and hornblende. On weathered surfaces, the granite varies in color between orange, dark brown and black.



Figure 21. Views of the Cross Creek Granite in outcrop. The left image shows a more orange-pink coloring, and the right image shows the dark grey color of the Cross Creek Granite as viewed from the west.

Diorite

The diorite unit in the field area (Fig. 22) is melanocratic; phaneritic in texture; medium-grained and contains biotite, quartz, plagioclase and hornblende. Magnetite is also present throughout these rocks, so caution was used when recording compass measurements in the study area. The diorite is about 70% dark minerals and 30% light minerals, with approximately 40% biotite, 30% hornblende, 20% plagioclase and 10% quartz. The weathered surface of the

diorite outcrops is dark gray. In some areas, light pink pegmatite dikes are common.



Figure 22. *Diorite unit in outcrop as viewed from the west.*

Gneiss

The gneiss unit (Fig. 23) in the study area is foliated and contains quartz, feldspar, plagioclase, biotite and hornblende. It is weakly mylonitic and migmatitic throughout the thesis area. Folds and sigmoidal shapes within the gneiss were observed (Fig. 23). On fresh surfaces, the gneiss is about 55% light minerals and



Figure 23. Views of the gneiss in outcrop. The left image is gneiss as viewed from the west, and the right image shows the texture of the gneiss including small, intrafolial folds.

45% dark minerals; the estimated percentage of each mineral is 35%

hornblende, 25% quartz, 20% feldspar, 10% plagioclase and 10% biotite. The unit weathers to brown-orange or a dark brown-gray color.

Pegmatites

Pegmatite bodies within the basement units are light pink rocks with potassium feldspar, quartz and biotite. In weathered outcrops, they appear light

brown to dark pink. Some pegmatite dikes also include large biotite crystals around 4 inches long and 2 inches wide (Figure 24).



Figure 24. *Biotite crystals in pegmatite dike.*

Sawatch Formation

The late Cambrian Sawatch Formation (Fig. 25) is a sandstone that is light tan on fresh surfaces and contains quartz grains that are medium- to fine-grained (1-0.1mm), well- rounded and well-sorted. The lithology could also be referred to as a quartzarenite. The base of the Sawatch Formation has a basal conglomerate (Fig. 26), with larger quartz fragments ranging from 10-30mm in size. Sedimentary structures observed included bedding and cross bedding. In the upper part of the Sawatch Formation the unit is brecciated in some areas.



Figure 25. *View of the Sawatch Formation in outcrop as viewed from the west along U.S. Highway 24.*



Figure 26. *Large quartz clast in the basal conglomerate in the Sawatch Formation.*



Figure 27. *Brecciation in Sawatch Formation*

Relationship of Rock Units

The diorite, gneiss and Cross Creek Granite contacts are often covered by debris. In some cases the contacts may be gradational. Along the Eagle River canyon, contacts between the units are mostly covered by debris between outcrops of the rocks that form cliffs in that area. The gneiss is the oldest unit in the area and the Cross Creek Granite batholith intruded into the gneiss and the diorite (Tweto et al., 1977). The units are also intruded by felsic dikes and pegmatites throughout the area (Fig. 28). The dikes range in width from 5-10



Figure 28. *Felsic dike within the Cross Creek Granite.*

inches to 1-2 feet. The dikes are common throughout the Paleoproterozoic units. Xenoliths of diorite are observed within the Cross Creek Granite, which indicates that the diorite is older than the granite (Fig. 29).



Figure 29. *Xenoliths of Diorite within Cross Creek Granite at Locality 4. The right part of the figure shows a close-up of the central xenolith.*

At the nonconformable contact between the basement and the Sawatch Formation, there is a paleocritical zone (Fig. 30) where the basement units were exposed and experienced weathering before deposition of the Sawatch Formation. No paleosols were observed because soil was not developed at this contact. The basement rocks at the contact are highly weathered and friable.



Figure 30. *Paleocritical zone and nonconformity between the basement rocks and the Sawatch Formation.*

CHAPTER 4

Structural Data and Initial Discussion

Introduction

Strike and dip was measured on 243 planar features, including joints, faults, bedding and foliation planes. Trend and plunge was measured on 40 linear features, including lineations on foliation planes and slickenlines on fault planes. Measurements of faults, joints and slickenlines were plotted on equal area stereographic projections. Planar and linear features with 10 measurements or more were also contoured with 1% area contour, which calculates how many points make up 1% of the total amount of data. Warmer contour colors indicate more data points, and for comparative stereograms the rainbow fill of the contours was removed for clearer comparison. A data table of all field measurements and locations can be found in the appendix.

Faults in the Study Area

Normal, thrust and strike-slip faults occur throughout the field area in both the basement and cover units. Evidence of faulting included slickenlines (Fig. 31), fault breccia, gouge and chatter marks (or steps). Strike and dip was measured on 60 faults throughout the study area. Of the 60 faults that were measured, 36 had a distinct fault type movement.



Figure 31. *Examples of slickenlines observed in the study area.*

Fault Descriptions

There are numerous faults located throughout the thesis area and examples of each type of fault in the area are described in the following section in greater detail (Fig. 32). In some locations, faults are continuous from the basement rocks into the Sawatch Formation, suggesting that they are late Cambrian or younger. Some faults had holes blasted from mining exploration. Unfortunately, there are few offset indicators to help quantitatively determine the offset.

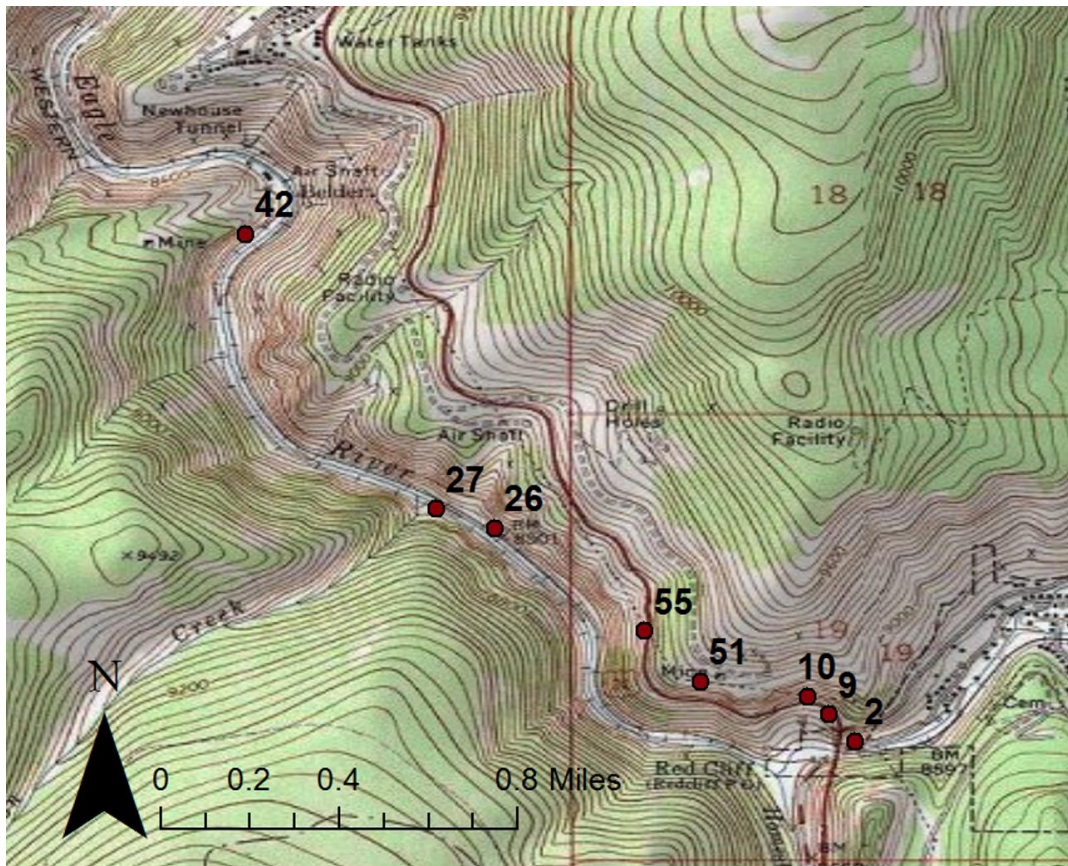


Figure 32. Topographic map of localities of fault examples throughout the study area.

The fault at Locality 2 (Fig. 33) is a normal fault within the basement units, and exhibited fault gouge. The fault at Locality 26 within the basement rocks

Normal Fault at Locality 2

Location: Below and East of Eagle River Bridge (Latitude: 39.5082 Longitude: -106.3755)

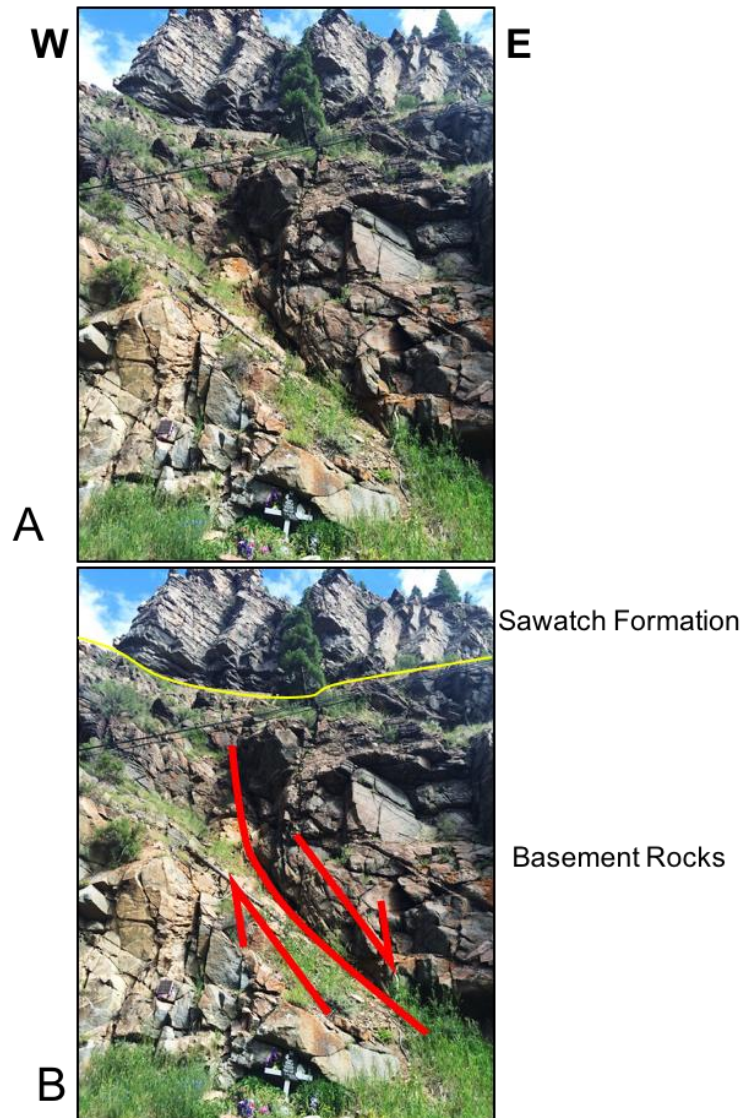


Figure 33. A: Picture of fault at Locality 2 as viewed from the south. **B:** Normal fault interpretation at Locality 2 with red line indicating fault plane and arrows indicating movement.

(Fig. 34) also exhibits normal fault movement. At locality 27 (Fig. 35) there is a fault within the basement rocks that has experienced left-lateral strike-slip

Normal Fault at Locality 26

Location: South of Sulphur Mine Gulch (Latitude: 39.5151 Longitude: -106.3876)

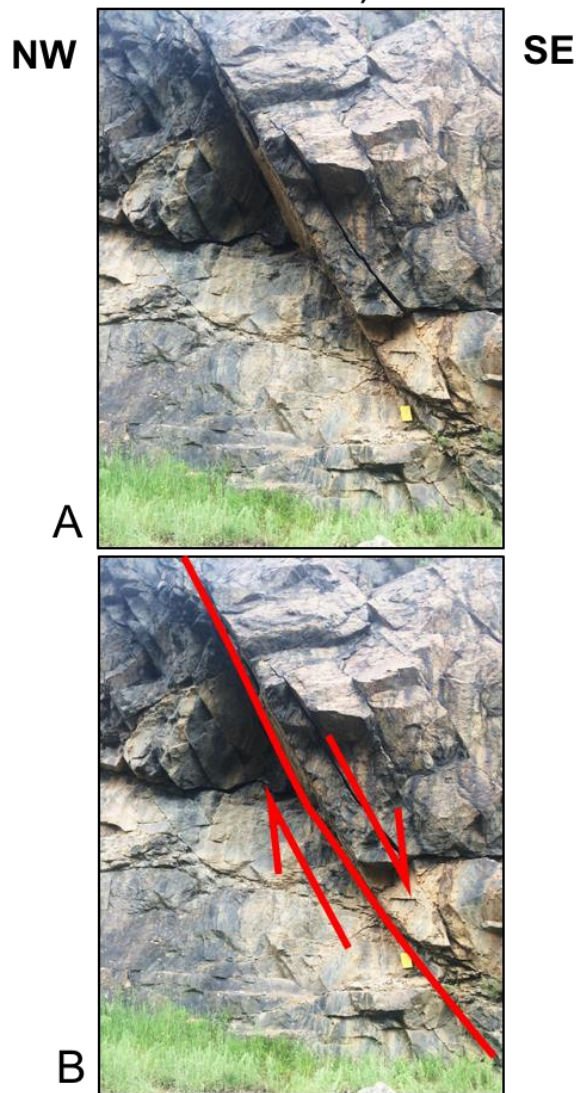


Figure 34. A: Picture of fault at Locality 26 as viewed from the southwest. **B:** Normal fault interpretation at Locality 26 with red line indicating fault plane arrows indicating movement.

Left-lateral Strike-slip Fault at Locality 27

Location: North of Sulphur Mine Gulch (Latitude: 39.5158 Longitude: -106.3890)

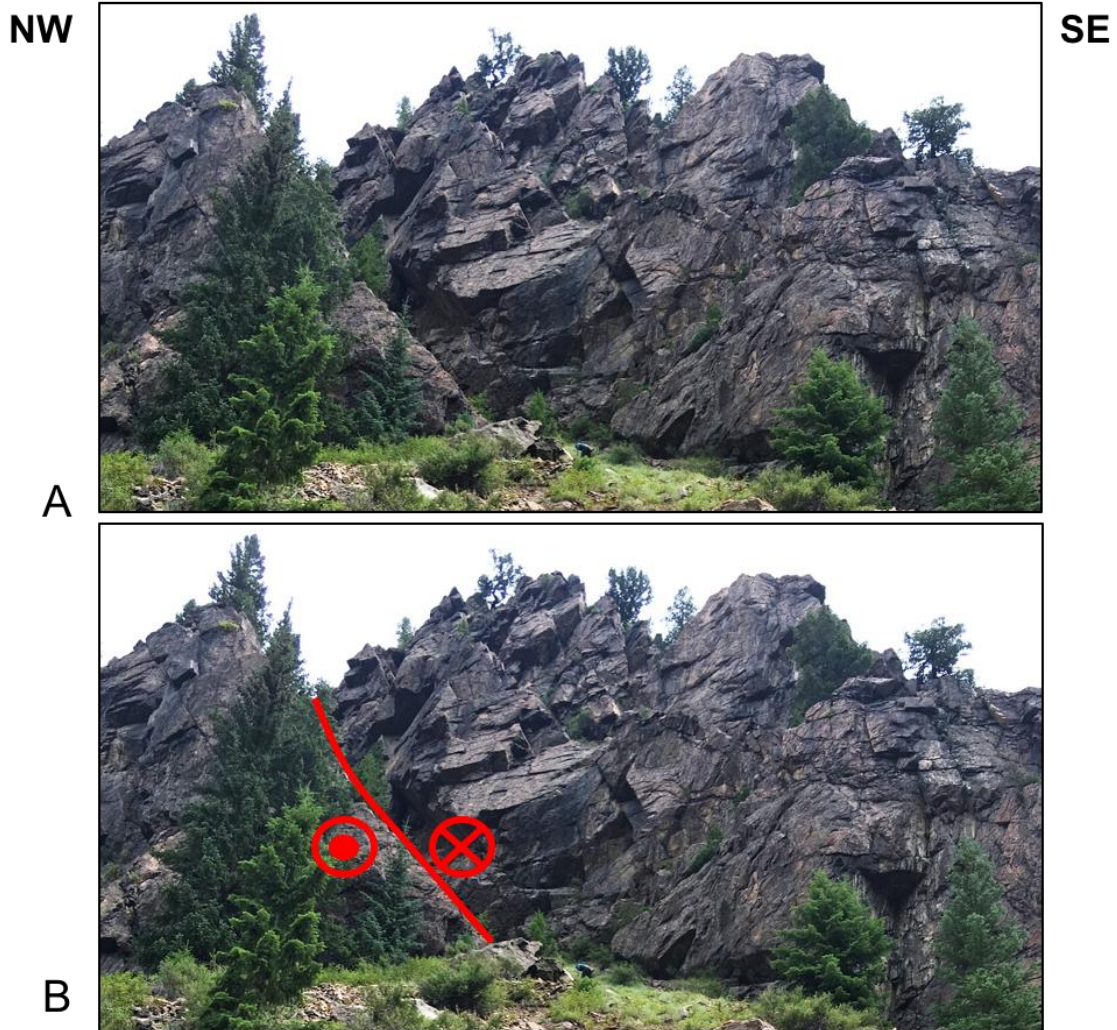


Figure 35. A: Picture of fault at Locality 27 as viewed from the southwest. **B:** Left lateral strike-slip fault interpretation at Locality 27 with the red line indicating the fault plane and symbols indicating relative movement.

movement. Within the basement units at Locality 42 there is a thrust fault that has a sigmoidal shape within the fault zone that indicates top to the southwest as viewed from the northwest (Fig. 36).

Thrust Fault at Locality 42

Location: South of Gilman Superfund Site (Latitude: 39.5243
Longitude: -106.3954)

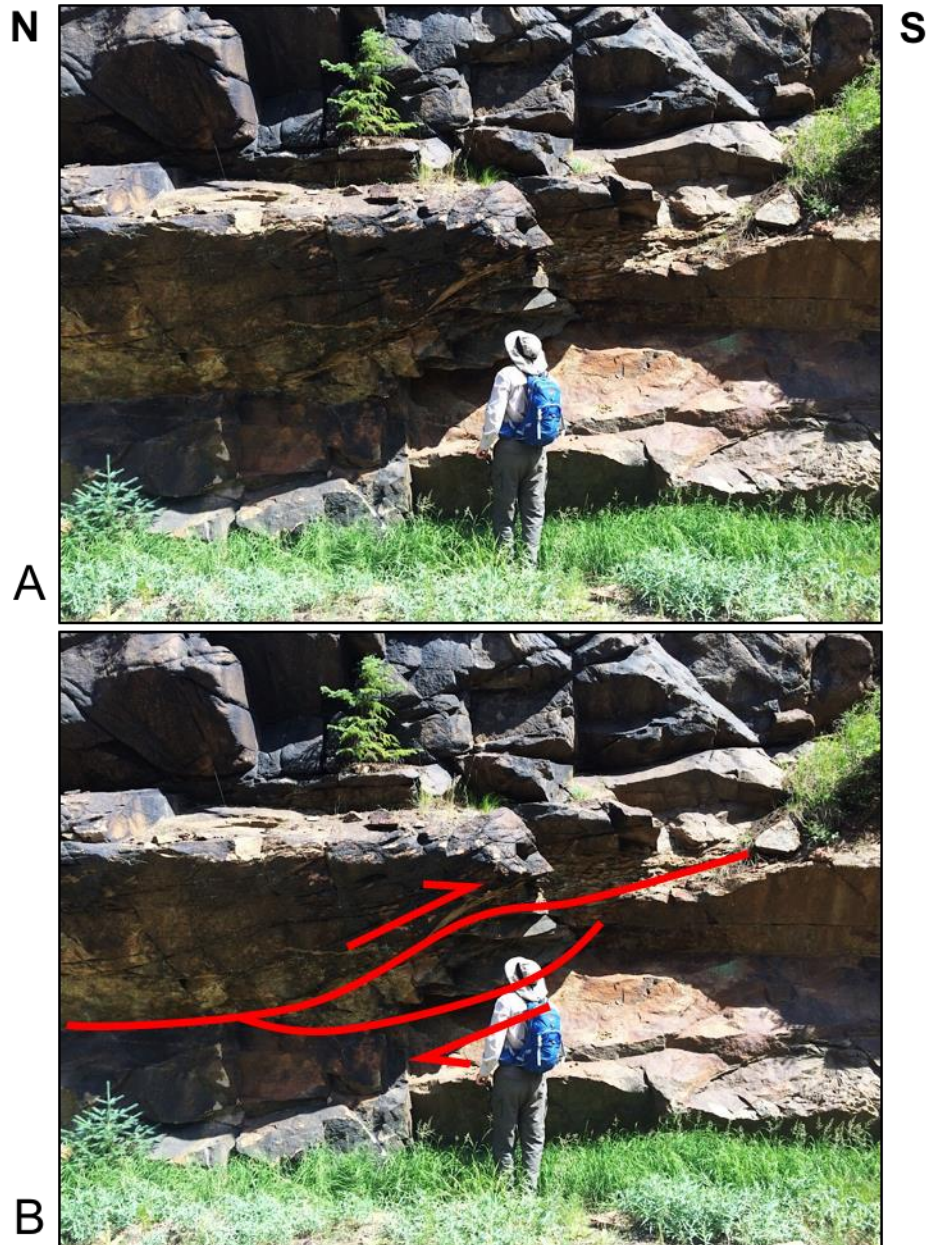


Figure 36. A: Picture of fault at Locality 42 as viewed from the west. **B:** Thrust fault interpretation at Locality 42 with red line indicating fault plane and arrows indicating movement.

North of the Eagle River bridge in the cliffs of the Sawatch Formation are faults that may be splay faults of a possible negative flower structure from strike-slip faulting (Fig. 37). There are five faults that are a part of this system. This

Faults at Locality 9

Location: North of Eagle River Bridge (Latitude: 39.5091 Longitude: -106.3766)

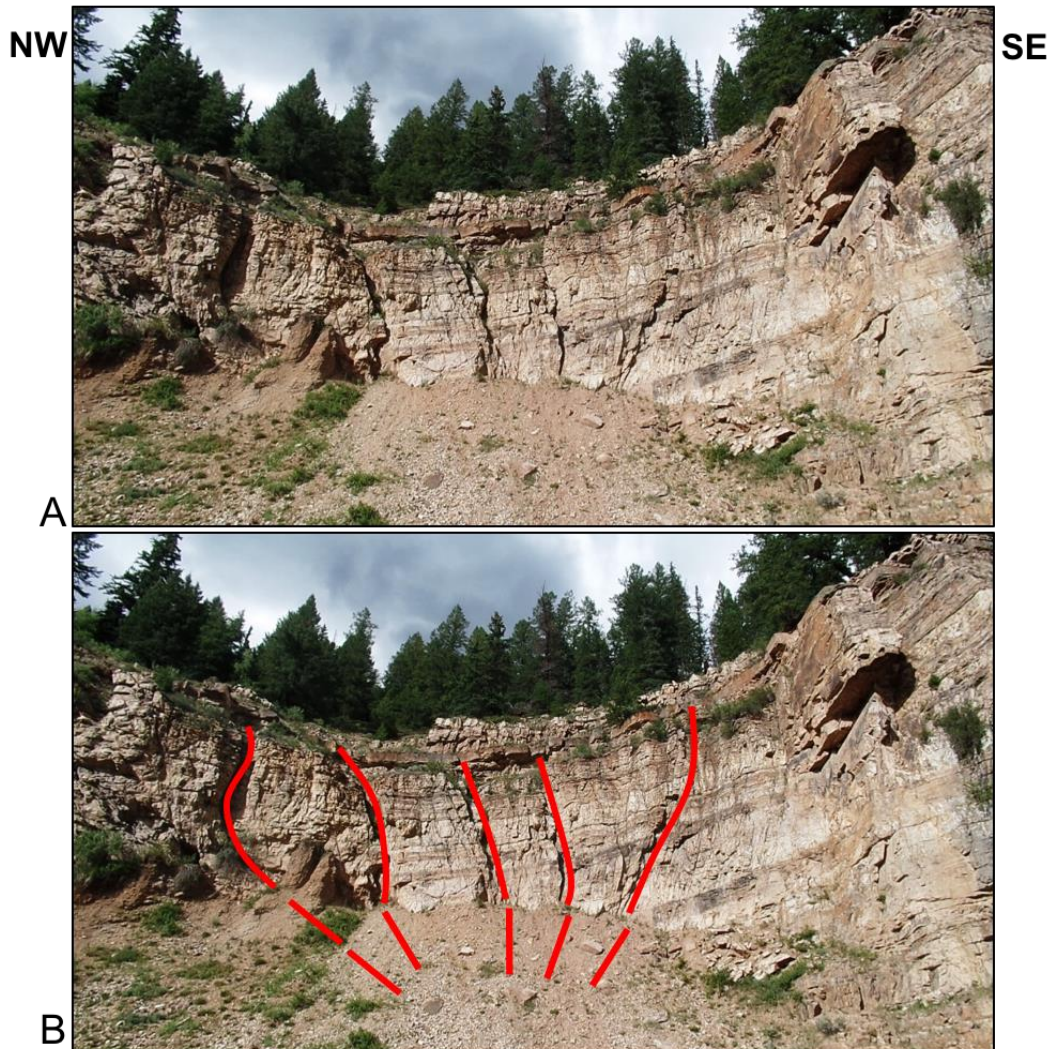


Figure 37. A: Picture of faults at Locality 9 as viewed from the southwest. **B:** Faults at Locality 9 with red lines indicating interpretation of a negative flower structure.

interpretation is based off of published flower structure models (Fossen, 2010). Approximately 100 feet north on U.S. Highway 24 from Locality 9 is a thrust fault at Locality 10 (Fig. 38). This thrust fault appears to have moved top to the west as viewed from the south. At Locality 51, within the Sawatch Formation there is a right lateral strike-slip fault (Fig. 39). At Locality 55 the fault movement that occurred in the sandstone blocks exhibits right-lateral strike-slip faulting (Fig. 40).

Thrust Fault at Locality 10

Location: North of Eagle River Bridge (Latitude: 39.5099
Longitude: -106.3773)

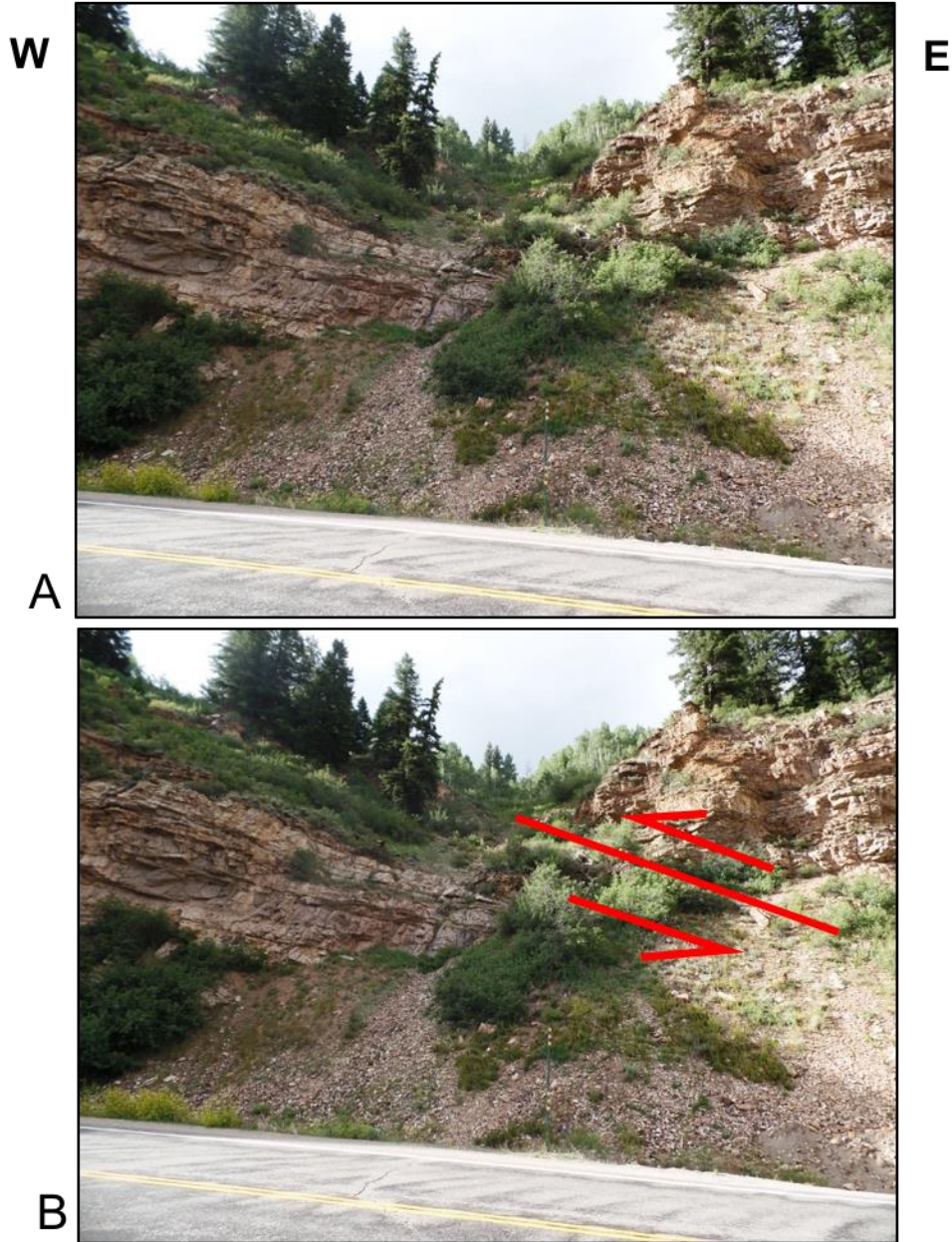


Figure 38. A: Picture of fault at Locality 10 as viewed from the south. **B:** Thrust fault at Locality 10 with a red line indicating fault plane and arrows indicating movement.

Right-lateral Strike-slip Fault at Locality 51

**Location: North of Eagle River Bridge Overlook (Latitude: 39.5097
Longitude: -106.3800)**

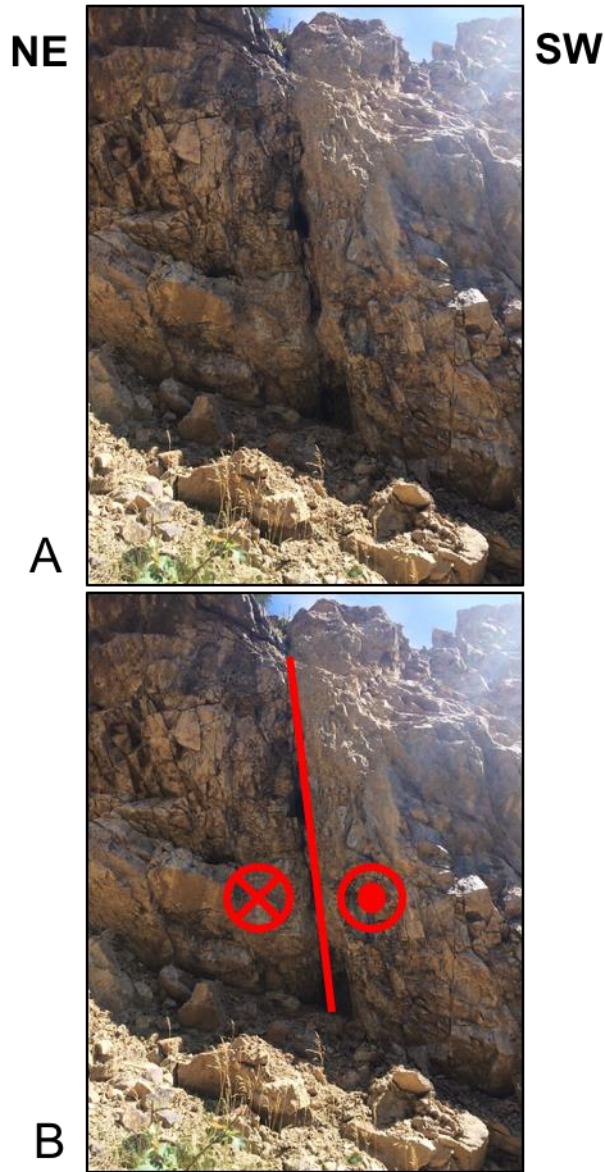


Figure 39. A: *Picture of fault at Locality 51 as viewed from the northwest. B:* *Right-lateral strike-slip fault at Locality 51 with a red line indicating fault plane and symbols indicating relative movement.*

Right-lateral Strike-slip Fault at Locality 55

**Location: North of Eagle River Bridge Overlook (Latitude: 39.5118
Longitude: -106.3826**

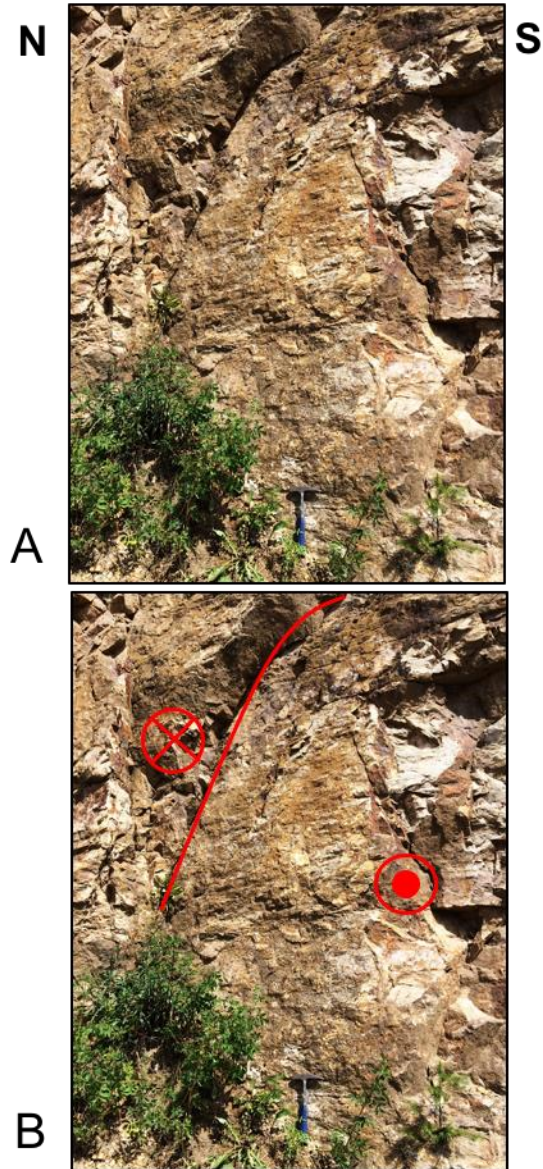


Figure 40. A: *Picture of fault at Locality 55 as viewed from the west at an angle to the fault plane. B:* *Right-lateral strike-slip fault at Locality 55 with a red line indicating fault plane and symbols indicating relative movement.*

Fault Types and Stereograms

Different fault types within the Paleoproterozoic basement and Sawatch Formation are represented in the following stereograms. Blue represents faults in the basement units and red represents faults within the Sawatch Formation. A circle encompassing the mean vector in some stereograms represents a 95% statistical confidence that the mean vector is located somewhere within that circle. The stereograms in this section are presented in order of left-lateral strike-slip faults, right-lateral strike-slip faults, normal faults and thrust faults.

A stereogram of left-lateral strike-slip fault data is shown in Figure 41. The mean vectors are represented by the larger blue and red points. There are eight left-lateral strike-slip faults within the basement units and two within the Sawatch Formation. Strike and dip is reported in azimuth measurements that were taken using the right-hand rule. Quadrant style measurements are also provided in parentheses, with all strikes relative to the northern quadrants. The strike and dip of the mean vector for the basement left-lateral strike-slip faults is 103° and 33° SW (N77W,33°SW). The strike and dip of the mean vector for the cover left-lateral strike slip faults is 040° and 76° SE (N40E,76°SE). The average northwest strike in the basement versus the northeast strike in the cover of these faults suggest that they were created by different stresses.

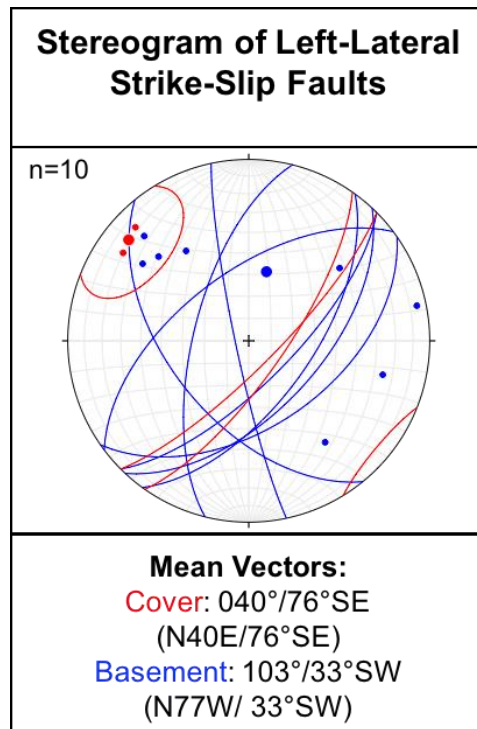


Figure 41. *Stereogram of left-lateral strike-slip faults in the basement and cover units. Mean vectors indicate the strike of the faults in the basement are oriented to the NW, while the mean vector for the faults in the cover indicate a NE strike.*

Right-lateral strike-slip stereogram data is shown in Figure 42. There is one right-lateral strike-slip fault within the basement units and four within the Sawatch Formation. The strike and dip of the mean vector for the basement right-lateral strike slip faults is 070° and 64° SE (N70E, 64°SE). The strike and dip of the mean vector for the cover right-lateral strike slip faults is 171° and 52° SW (N9W, 52° SW). There are only 5 measurements, but these faults exhibit strikes that are northeast (in the basement) and northwest (in the cover). There is probably nothing to suggest that there is any relationship between right-lateral strike-slip

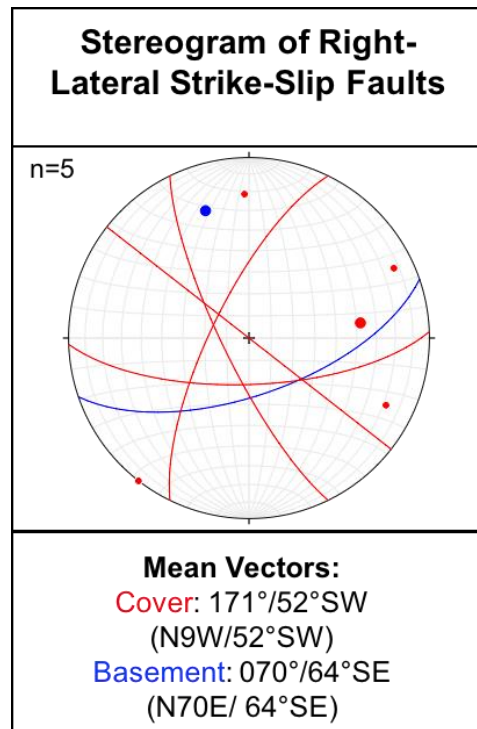


Figure 42. *Stereogram of right-lateral strike-slip faults in the basement and cover units. The mean vector indicates the strike of the fault in the basement is oriented to the NE, while the mean vector for the faults in the cover indicate a NW strike.*

faults in the basement and in the cover rocks.

Normal fault stereogram data is shown in Figure 43. There are 12 normal faults within the basement units and one within the Sawatch Formation. The strike and dip of the mean vector for the basement normal faults is 046° and 49° SE (N46E, 49°SE). The strike and dip of the mean vector for the cover normal fault is 058° and 55° SE (N58E,55°SE). The mean vectors for normal faults in the study exhibit an average northeast strike in the basement and cover units.

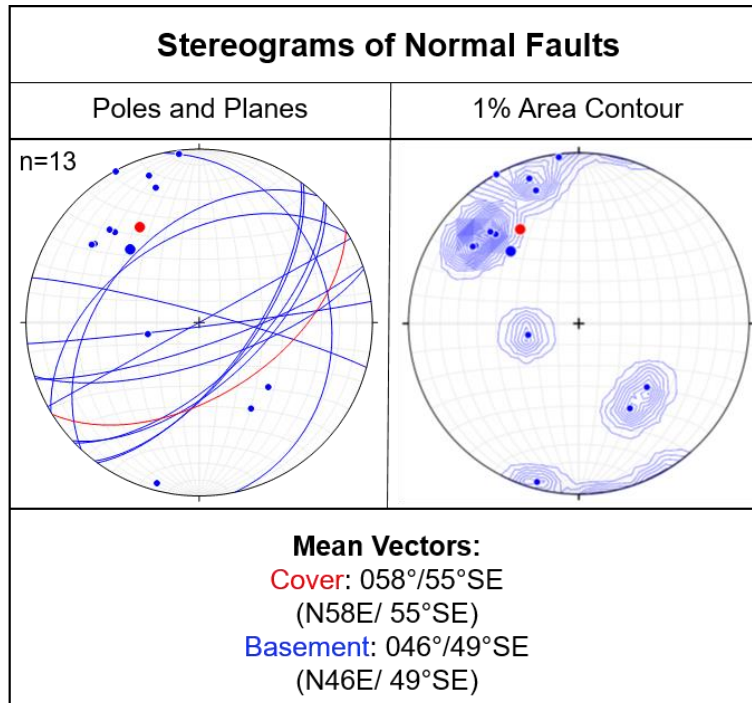


Figure 43. Stereogram of normal faults in the basement and cover units. The mean vectors indicate the strike of the faults in the basement and cover are oriented to the NE.

Thrust fault data in the study area is shown in Figure 44. There are six thrust faults within the basement units and two within the Sawatch Formation. The strike and dip of the mean vector for the basement thrust faults is 071° and 28° SE (N71E,28°SE). The strike and dip of the mean vector for the cover thrust faults is 347° and 28° NE (N13W, 28° NE). Thrust faults in the basement have an average strike to the northeast and in the cover to the northwest, this also suggests that the basement and cover rocks experienced different stresses.

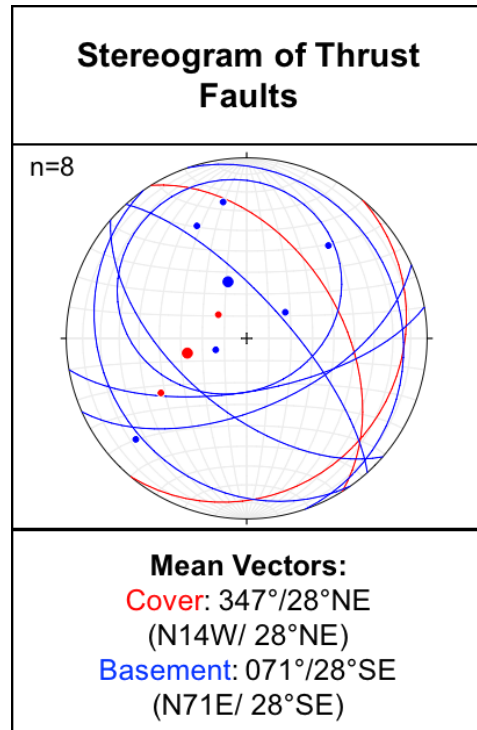


Figure 44. *Stereogram of thrust faults in the basement and cover units. The mean vector indicates the strike of faults in the basement is oriented to the NE, while the mean vector for the faults in the cover indicate a NW strike.*

Information from the stereograms in Figures 41-44 is compiled into Table 1. Within the basement, all fault types strike on average to the NE except for left-lateral strike slip faults which strike to the NW on average. In the cover, left-lateral and normal faults strike NE on average and the right-lateral strike-slip faults and thrust faults on average strike to the NW. Both the basement and cover units contain faults oriented to the northeast and northwest. This suggests that there may have been different directions of stresses acting on these units at different periods of time.

Table 1. Summary of fault data from stereograms in figures 41-44.

Fault Type	Unit	n =	Mean Vector Strike and Dip
Left-lateral strike slip	Cover	2	040°/76°SE (N40E/76°SE)
	Basement	8	103°/33° SW (N77W/ 33°SW)
Right-lateral strike slip	Cover	4	171°/52° SW (N9W/52°SW)
	Basement	1	070°/64° SE (N70E/ 64°SE)
Normal	Cover	1	058°/55° SE (N58E/ 55°SE)
	Basement	12	046°/49° SE (N46E/ 49°SE)
Thrust	Cover	2	347°/28° NE (N13W/ 28°NE)
	Basement	6	071°/28° SE (N71E/ 28°SE)

Slickenlines

Measurements were made on slickenlines on 40 different fault planes in the basement and cover units (Fig. 45). There are 33 slickenline measurements within the basement units and seven within the Sawatch Formation. Plunge and bearing of the mean vector for the basement slickenlines is 86° and 172° (86°, S8E). The plunge and bearing of the mean vector for the cover slickenlines is 14° and 248° (14°, S68W). The slickenline stereograms (Fig. 45) show different

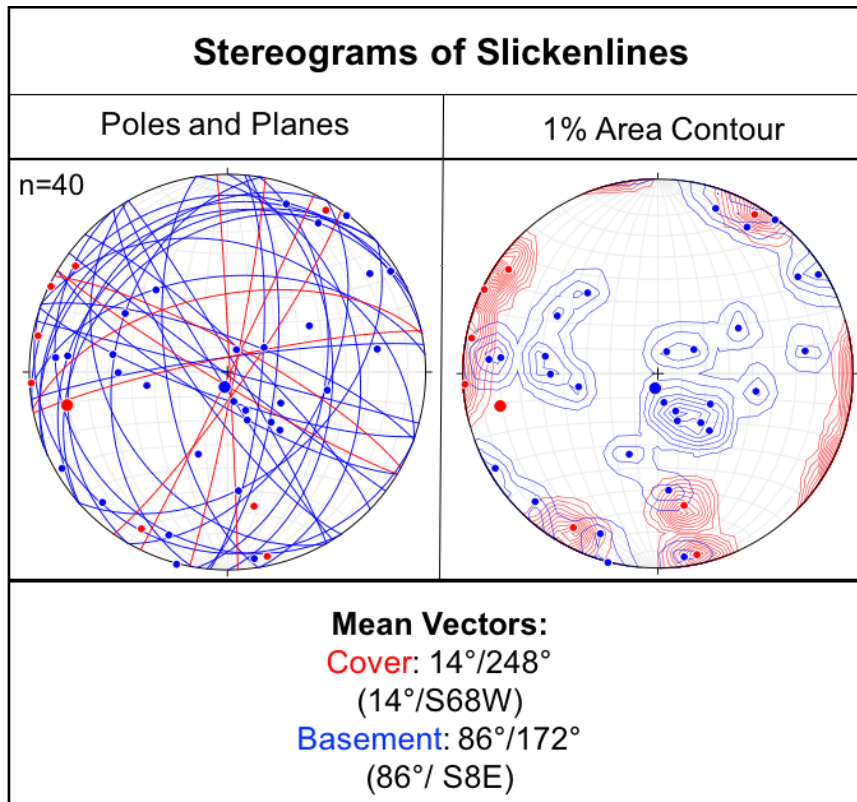


Figure 45. Stereogram of slickenlines in the basement and cover units. The mean vector indicates the trend of slickenlines in the basement is oriented to the SE, while the mean vector for the slickenlines in the cover indicate a SW trend.

orientations in the basement and cover. A majority of slickenline measurements in the basement units are grouped in the center of the stereogram indicating that they are sub-vertical, whereas slickenlines measured in the cover are located towards the edges of the stereogram indicating that they are more shallow dipping.

Basement Units Separated

Stereograms of the basement rocks are separated in this section into the diorite, Cross Creek Granite and gneiss, the units that constitute the basement in the study area. The joints and faults within the units are represented in stereograms (Figs. 46-48).

The diorite stereogram data is shown in Figure 46. The fault data mean vector has a strike of 122° and a dip of 8° SW (N58W, 8° SW). The joint data mean vector has a strike of 094° and a dip of 20° SW (N86W, 20° SW). Although the faults within the diorite have an average strike to the northwest, there are groupings of data observed within the stereogram that also exhibit a northeast strike. Stereograms of joints within the diorite exhibit groups of data that have orientations to the northwest and the northeast.

The Cross Creek Granite stereogram data is shown in Figure 47. The mean vector for faults in the Cross Creek Granite has a strike of 041° and dip of 34° SE (N41E, 34° SE). The mean vector for the joints in the Cross Creek Granite has a strike of 092° and dip of 19° SW (N88W, 19° SW). The joint patterns within the Cross Creek Granite also exhibit distinct groups of data that are striking in different orientations.

The stereogram data for the gneiss unit is shown in Figure 48. The mean vector for the faults within this unit has a strike of 70° and a dip of 61° SE (N70E,

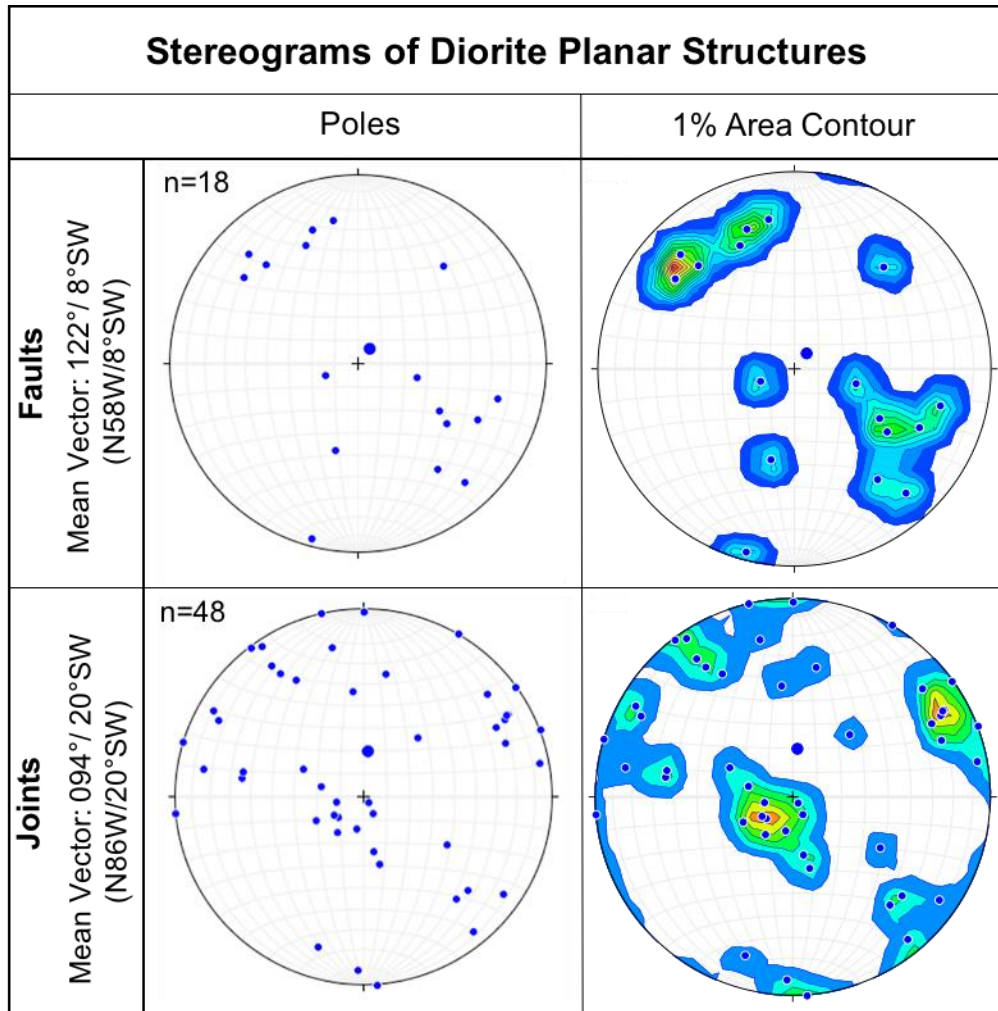


Figure 46. Stereogram data of faults and joints in the diorite. The mean vector of faults and joints indicates the average strike is oriented to the NW.

61°SE). For the joints, the mean vector has a strike of 130° and dip of 31° SW (N50W, 31°SW). Faults within the gneiss are primarily northeast striking and joints within the gneiss exhibit strikes to both the northwest and northeast.

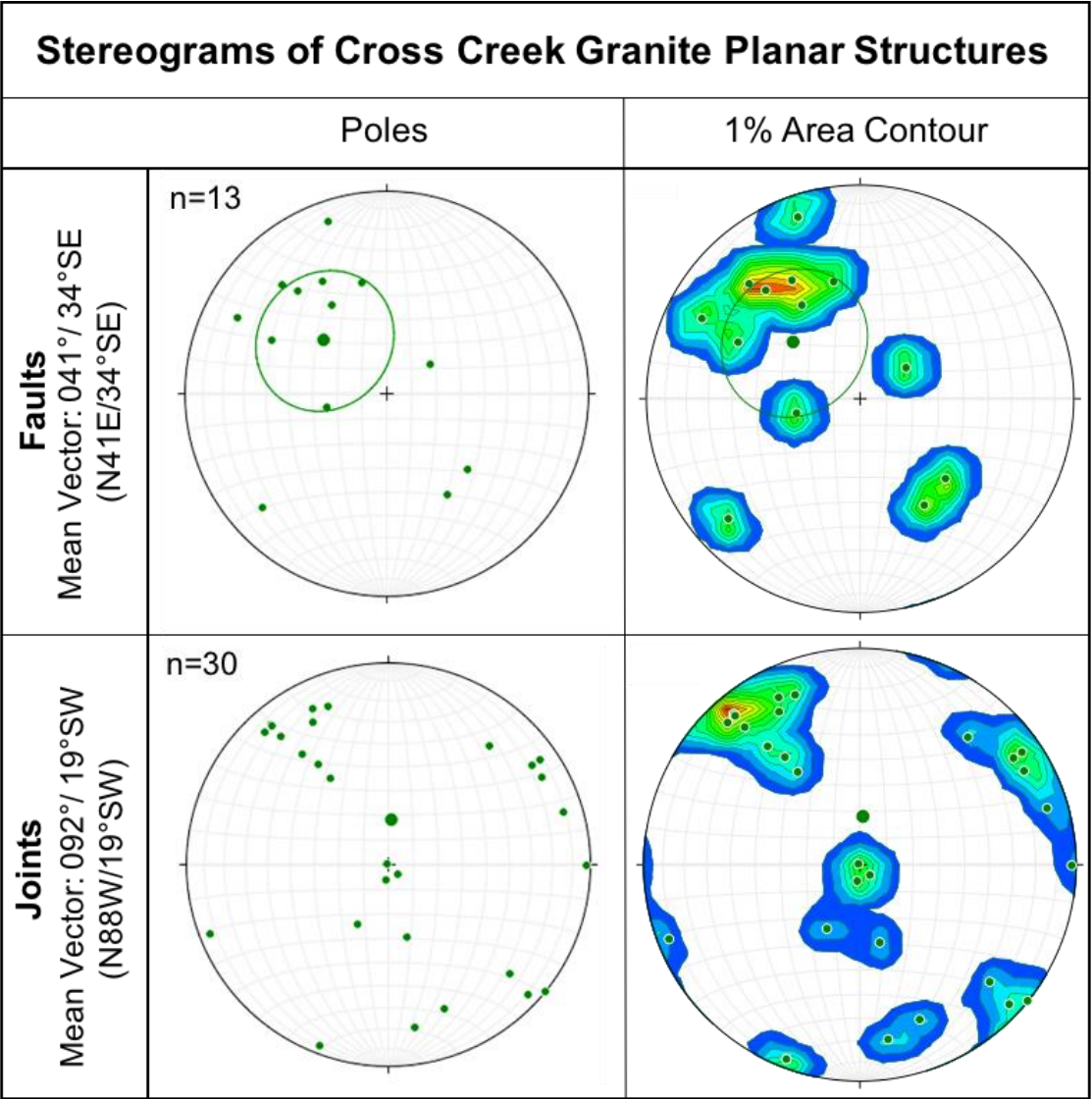


Figure 47. Stereogram data of faults and joints in the Cross Creek Granite. The mean vector of faults indicates the average strike is oriented to the NE, while the mean vector for the joints indicate a NW strike.

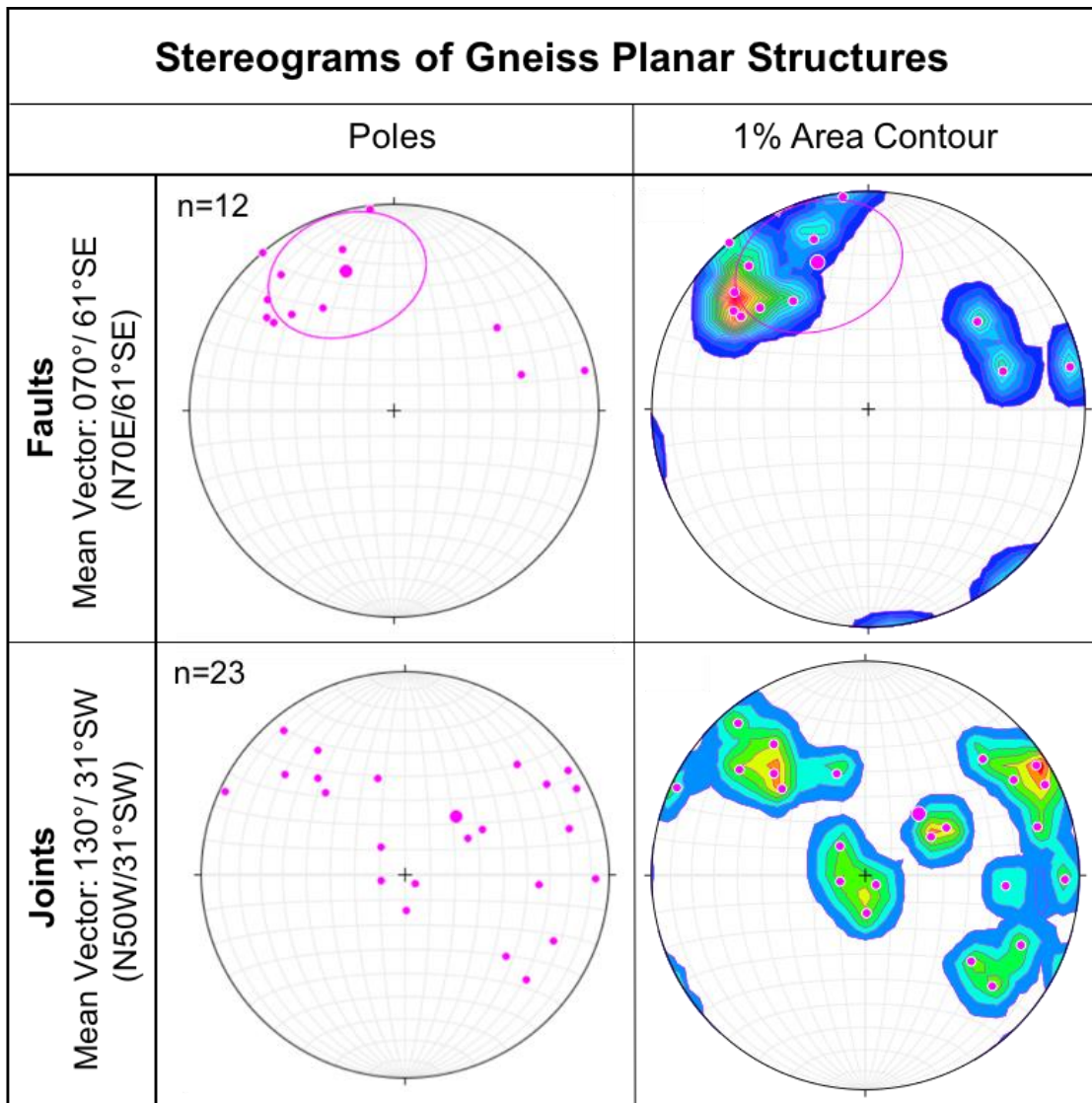


Figure 48. Stereogram data of faults and joints in the gneiss. The mean vector of faults indicates the average strike is oriented to the NE, while the mean vector for the joints indicate a NW strike.

Information from the stereograms in Figures 46-48 is compiled into Table 2. In the three basement units overall, the faults strike to the NE, with exception of faults in the diorite that strike to the NW. The joints on average strike to the NW, except the joints in the diorite, which primarily strike to the NE.

Table 2. Summary of basement unit data from stereograms in figures 46-48.

Unit Type	Structure Type	n =	Mean Vector Strike and Dip
Diorite	Faults	18	122°/ 8°SW (N58W/8°SW)
	Joints	48	094°/ 20°SW (N86W/20°SW)
Cross Creek Granite	Faults	13	041°/ 34°SE (N41E/34°SE)
	Joints	30	092°/ 19°SW (N88W/19°SW)
Gneiss	Faults	12	070°/ 61°SE (N70E/61°SE)
	Joints	23	130°/ 31°SW (N50W/31°SW)

Basement Structures

In the stereograms in Figure 49, the three units of basement rocks are compiled together and exhibit all of the planar data for faults and joints. The mean vector for faults in the basement units has a strike and dip of 064°, 32° SE (N64E, 32°SE). The mean vector for the joints in the basement units has a strike and dip of 107°, 22° SW (N73W, 22° SW). The 1% area contour stereogram of all faults in the basement shows a large grouping of data that indicates a northeast strike. Joints in the basement units exhibit multiple groups of data with different structural trends.

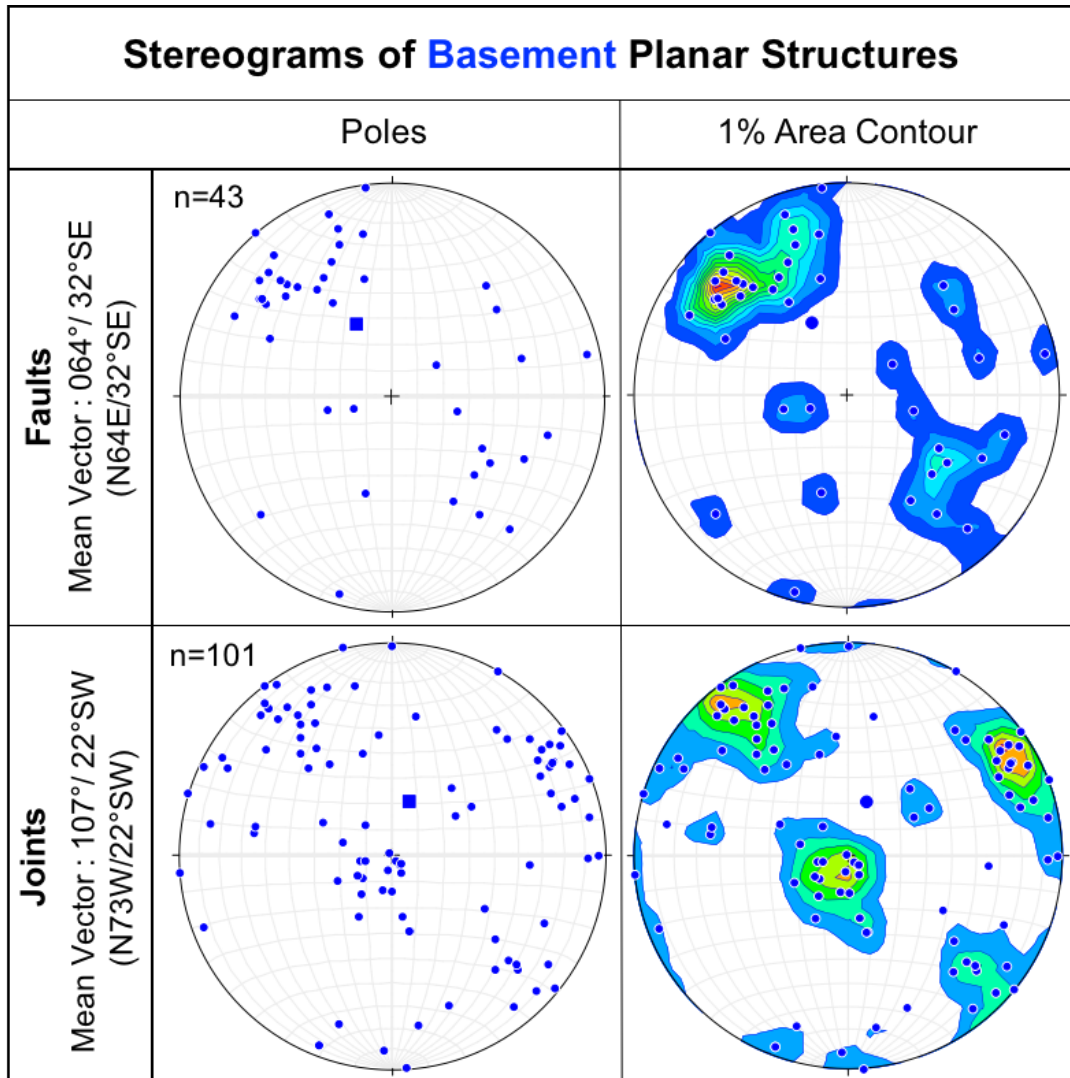


Figure 49. Stereogram data of faults and joints in the basement. The mean vector (larger blue squares and points) of faults indicates the average strike is oriented to the NE, while the mean vector for the joints indicate a NW strike.

Cover Structures

Stereograms of planar data from the Sawatch Formation are shown in

Figure 50. The mean vector for the faults had a strike of 042° and dip of 33° SE

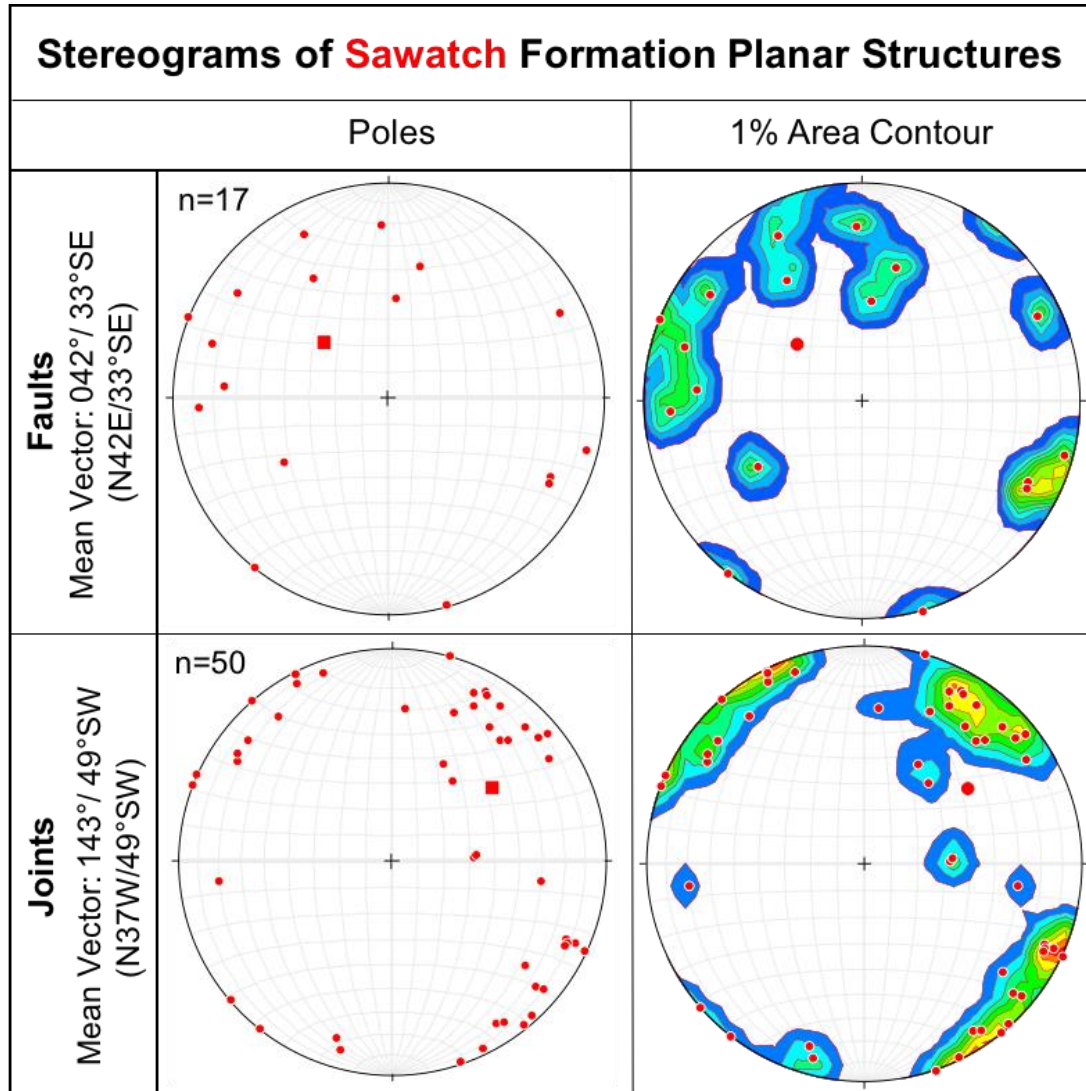


Figure 50. Stereogram data of faults and joints in the Sawatch Formation. The mean vector (larger red squares and points) of faults indicates the average strike is oriented to the NE, while the mean vector for the joints indicate a NW strike.

(N42E, 33°SE). The mean vector for the joints in the Sawatch Formation had a strike of 143° and dip of 49° SW (N37W, 49°SW). The distribution of fault data in the Sawatch Formation is variable, but the contours of that data exhibit that they have an orientation striking to the northeast. Joints within the Sawatch Formation also exhibit strike orientations that are northwest and northeast. These trends are consistent with joint data within the basement units as well.

Information from the stereograms in Figures 49-50 is compiled into Table 3. In the basement and cover the faults strike on average to the northeast and the joints on average strike to the northwest (though there is more variability in the orientation of the joints).

Table 3. Summary of basement and cover planar data from stereograms in figures 49 and 50.

Unit Type	Structure Type	n =	Mean Vector Strike and Dip
Basement	Faults	43	064°/ 32°SE (N64E/32°SE)
	Joints	101	107°/ 22°SW (N73W/22°SW)
Cover	Faults	17	042°/ 33°SE (N42E/33°SE)
	Joints	50	143°/ 49°SW (N37W/49°SW)

Basement and Cover Structures

The stereograms from figures 49 and 50 were combined in Figure 51 to

allow a comparative analysis of the basement and cover structures. The mean vectors of the faults from the Paleoproterozoic units (blue square and dot) and the Cambrian Sawatch formation (red square and dot) are close in their orientations and both strike to the NE. The mean vectors of the joints are not as

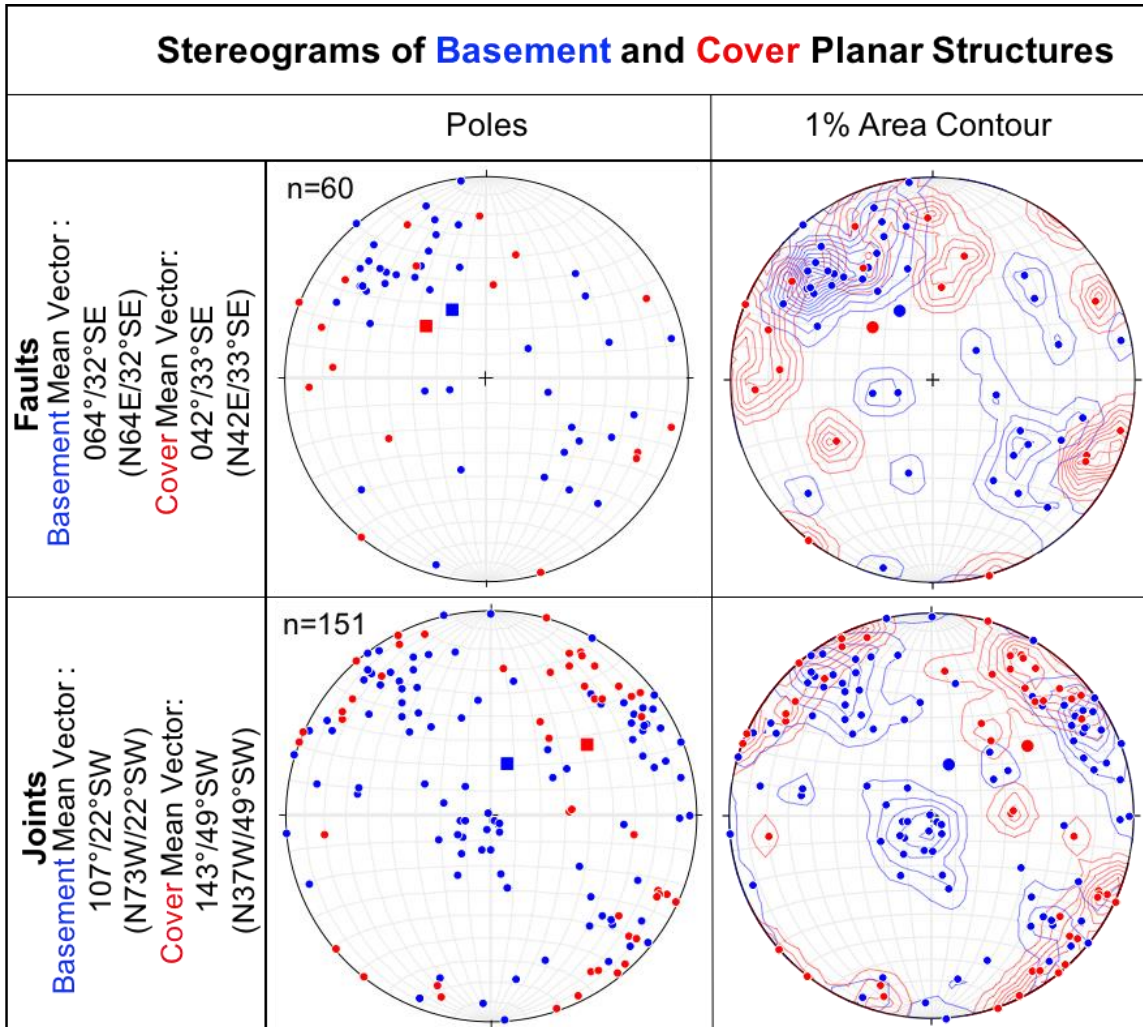


Figure 51. Stereogram data compiled from Figures 46 and 47 for comparative analysis of faults and joints in the basement and cover. The mean vectors of faults indicate the average strike is oriented to the NE, while the mean vectors for the joints indicate a NW strike.

closely oriented, but they both strike to the NW.

In Figure 51, the stereogram of faults in the basement and in the Sawatch Formation shows that the faults are closely correlated. This is indicated by mean vector values of 064° , 32° SE (N64E, 32° SE) for basement faults and 042° , 33° SE (N42E, 33° SE) for Sawatch Formation faults. This suggests that stresses that created faults in the basement and cover rocks may have had similar orientations. The stresses may have been active at different times, but had the same orientation. This orientation may be related to accretion of crustal provinces onto Laurentia during the Proterozoic (Karlstrom et al., 1998). Accretions during orogenies of this time like the Yavapai and Mazatzal would have created northeast structural trends created in the rocks within the study area (Karlstrom et al., 1998). It may be possible that this orientation continued to influenced structures in the future (Stone, 2002).

An alternate interpretation is that the predominant NE structural trend of the basement units influenced the development of a similar NE trend in the overlying Sawatch strata, even though stresses acting on the Sawatch Formation during the Phanerozoic probably did have a different orientation. Thus, the influence of the NE structural trend of the basement rocks may have exceeded the effect of later stress directions and have been the deciding factor in the development of a NE orientation in the cover rocks.

The stereograms of joints likewise shows a correlation, though there is a

group of joints in the basement rocks that do not have any corresponding joints in the Sawatch Formation (these are the poles located in the center of the stereogram, which will be discussed later). The mean vector values plot relatively close together with the mean vector values for joints in the basement being 107° , 22° SW (N73W, 22° SW) and the mean vector for joints in the Sawatch Formation is 143° , 49° SW (N37W, 49° SW).

CHAPTER 5

Further Discussion

Structural Trend Comparisons

Dip-slip and strike-slip faults occur in both the basement units and the Sawatch Formation. There were 15 faults with strike-slip movement measured and 21 faults measured with dip-slip movement in the study area. Forty-three faults were measured in the basement and 17 measured in the Sawatch Formation. Faults in the basement and cover on average strike to the northeast. There were 101 joints measured in the basement units and 50 joints measured in the Sawatch Formation. The overall strike of the joints in the basement and cover is oriented to the northwest.

There are groupings of planar measurements within the stereograms of the basement and Sawatch Formation in Figures 49, 50 and 51. In Figure 52, the stereogram of faults in the basement and cover rocks shows a large grouping of poles with an orientation striking to the northeast. This overall northeast strike of the faults throughout the thesis area may indicate that the orientation has been influenced by the structural trends formed in the crust during Proterozoic deformational events and accretions of continental lithosphere. The accretion of crustal provinces onto Laurentia during the Proterozoic initially created this

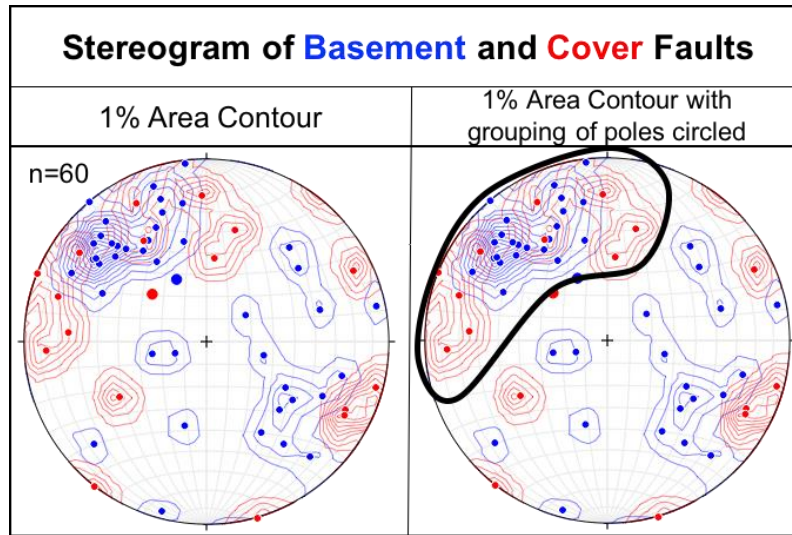


Figure 52. *Stereogram data of faults in the basement and cover. Contouring and black outline on the right stereogram of poles shows a majority of poles that strike to the NE.*

structural orientation (Karlstrom et al., 1998). The northeast orientation is thought to have influenced geologic features throughout geologic time (Stone, 2002). Geologic features close to the study area that exhibit a northeast striking orientation include the Colorado Mineral Belt, Homestake shear zone and other shear zones proximal to the study area like the Slide Lake shear zone and Independence Pass shear zone (Shaw et al. 2007; Lee et al., 2012).

Stereograms of joint orientations in the basement and cover rocks revealed 4 groupings of poles labeled A, B, C and D in Figure 53. Groups D and B have an orientation that is striking to the northwest (which is the average strike of all joints in the basement and cover). The poles within group B are only found within the basement, and do not correlate with any cover measurements. These joints exhibit a northwest strike and were probably created by stresses in the

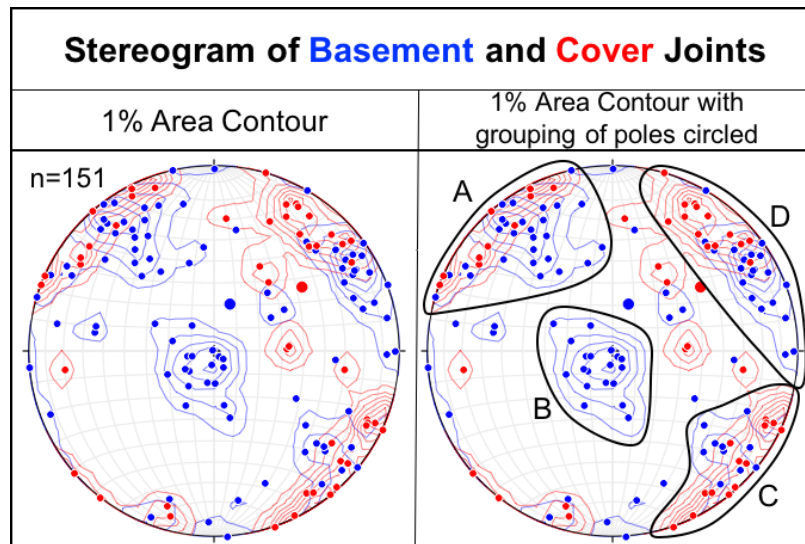


Figure 53. *Stereogram data of joints in the basement and cover. Contouring and black outlines on the right stereogram of poles shows groups of poles that strike to the NW and the NE.*

Paleoproterozoic, because they only occur within the basement units. It is also possible that joints in the Sawatch with this orientation were not found simply because the accessible areas of the Sawatch Formation are smaller than those of the basement units in the study area.

Groups A and C in Figure 53 exhibit a northeast striking orientation. These joints, which occur in both basement and cover rocks, have the same orientation as older structural trends created during the Proterozoic and the assembly of continental lithosphere (similar to the overall fault orientation in the study area).

The grouping of basement and cover poles in D that exhibit a northwest strike may be features associated with Ancestral Rockies and/or Laramide deformation. Overall, Laramide age geologic structures (like the Sawatch Range

anticlinorium) exhibit an orientation that trends north-south and northwest-southeast; these structural trends were created from compressive σ_1 stresses during the Laramide orogeny that were oriented to the northeast-southwest (Stone, 2002).

Some of the structures within the basement and cover that have a northeast striking orientation in the study area could have resulted in part from reactivation of basement faults during different deformation events. The previously existing structures that were created during the Paleoproterozoic may have been reactivated and influenced fault movement in the overlying rocks during uplift of the Sawatch Range in the Laramide orogeny. Normal faults observed in the basement rocks in the area may be reactivated reverse or thrust faults that were originally created by compression during the accretion of crust in the Paleoproterozoic. Further research on reactivation would be useful to determine whether structures in the area have experienced this process.

In summary, northeast and northwest striking structures observed throughout the study area could be a representation of a variety of structural orientations created by multiple deformational events throughout geologic time (Fig. 54). The creation of the northeast striking structures was formed from structural trends created from the assembly of continental lithosphere of Laurentia (Karlstrom et al., 1998). Deformation of Laurentia occurred throughout the Proterozoic. The Sawatch Formation was deposited in the late Cambrian

(Kirkham et al., 2011). In the Pennsylvanian, the uplift of intracratonic blocks and the creation of the Ancestral Rocky Mountains occurred (Kluth, 1986). Although the deformational processes that created the uplift are debated, the uplifts are thought to have had a north-northwest trend. Beginning ~70 Ma the Laramide orogeny uplifted basement-cored ranges that were oriented to the northwest-southeast and north-south (Weil et al., 2016). This sequence of events is depicted in Figure 54.

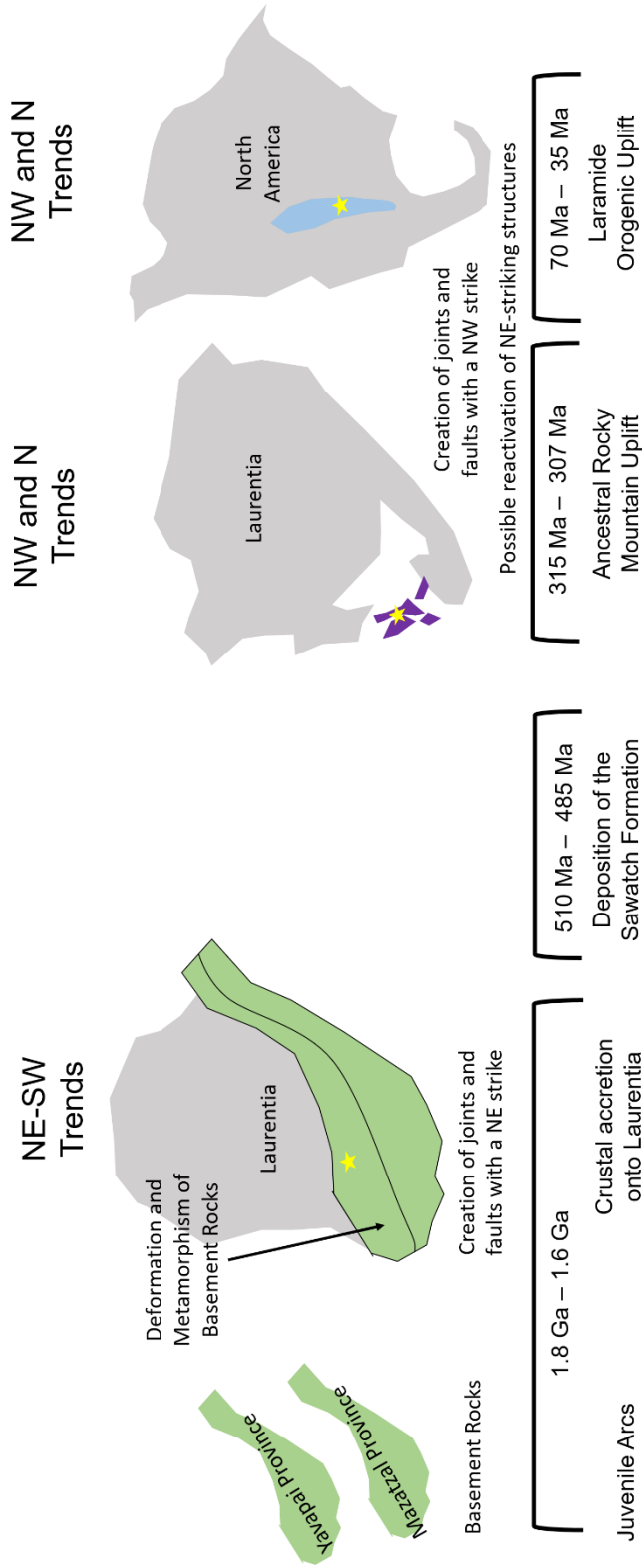


Figure 54. Illustration of tectonic and geologic events and associated structural trends relevant to the study area. Colored shapes represent uplifts in relation to Laurentia or North America. The green shapes are representative of crustal material that accreted onto Laurentia, purple shapes represent Ancestral Rocky Mountain uplifts and blue represents the Laramide orogenic uplifts. The yellow star represents the study area location. Note the change in structural orientation over time from the NE-SW during the Proterozoic to NW-SE and N-S in the Phanerozoic. These structural trends are represented by the structures observed in the study area.

CHAPTER 6

Conclusions

Structural analysis of basement rocks and the nonconformably overlying Sawatch Formation in the study area help reveal the geologic history of the area. A variety of fault type movements (dip-slip and strike-slip) was observed in the study area. Measurements of 60 faults and 151 joints throughout the study area revealed that the majority of faults have an average strike to the northeast and majorities of joints have an average strike to the northwest. A smaller group of joints have a northeast strike. A comparative analysis of the structures observed in this research with previously published works helps to constrain the relationship between orientation and tectonic deformational events in this area.

Geologic structures with a northeast strike could have inherited this orientation from structural trends that were created during the lithospheric accretion of Laurentia (Karlstrom et al., 1998). There are other geologic features that exhibit this orientation including: the Colorado Mineral Belt, Homestake shear zone, Independence Pass shear zone and Slide Lake shear zone (Shaw et al. 2007; Lee et al., 2012). Structures with a northwest orientation could be associated with Laramide orogenic deformation (Weil et al., 2016).

Multiple deformation events in this region have created the structures present in the study area (Fig. 50). A timeline of these events (also represented

in Figure 54) includes: during the Proterozoic, accretion of crustal materials onto Laurentia and multiple orogenic events established a northeast structural trend (Whitmeyer et al., 2007; Karlstrom et al., 1998). This created the joints and faults that have a northeast strike in the study area. During the late Cambrian, the Sawatch Formation was deposited over the basement rocks (Kirkham et al., 2011). North and northwest striking uplifts were created during Ancestral Rocky Mountain uplift in the Pennsylvanian (Chapin et al., 2014; Kluth, 1986). Joints and faults with a northwest orientation could have been created at this time. During the late Cretaceous (~70 Mya), flat slab subduction of the Farallon plate underneath the North American craton created an uplift of basement-cored ranges during the Laramide orogeny that have an overall orientation of northwest-southeast and north-south (Weil et al., 2016). This also created joint and faults in the study area that have a northwest strike. During either, or both, the Ancestral Rockies uplift or the Laramide orogeny, preexisting structures in the basement rocks may have been reactivated and caused development of the northeast trend seen in multiple structures in the overlying Sawatch Formation.

The structures within the study area exhibit both northeast and northwest orientations and these data add further understanding of the geologic history of the structures in this part of the Sawatch Range.

A timeline of events discussed above is presented in the following section.

Timeline of Deformation

- ~1.8-1.6 Ga: Crustal accretions onto Laurentia creates a NE-SW structural trend. NE striking joints and faults are created at this time.
- ~510-485 Ma: Deposition of the Sawatch Formation
- ~315-307 Ma: Ancestral Rocky Mountain uplift and creation of a north to NW trend. Structures with a NW trend could have been created at this time.
- ~70 Ma: Laramide orogeny also creates a NW structural trend and creates joints and faults with a NW striking orientation.
- Possible reactivation of basement structures during the Ancestral Rocky Mountain uplift and/or Laramide orogeny also creates northeast striking structures in the cover rocks.

Future Research

This area would benefit from continued research including: small scale detailed mapping and petrologic studies to delineate the nature and relationships of units in the Paleoproterozoic basement and detailed study of pegmatites and their orientations would enhance understanding of the basement units and mineralization patterns. Reactivation tendency analyses of structures in this area would possibly help to determine whether structures in the area have experienced this process. Remote sensing analyses of the lineaments in this

area would further enhance the understanding of the relationships between structures and the orientation of the lineaments in this area.

An engineering geology assessment of rockfall hazards from the Sawatch Formation along U.S. Highway 24 could give insight into hazard mitigation along the highway for increased safety in this section of mountainous highway.

Structural analyses of the northwestern side of the Sawatch Range would be beneficial in comparing structural styles on either side of the range. Investigating the orientation of structures on the northwest side of the range to determine if they exhibit the same patterns that have been found within the study area would be useful.

REFERENCES CITED

- Allen, J. L., 2005, A multi-kilometer pseudotachylyte system as an exhumed record of earthquake rupture geometry at hypo central depths (Colorado, USA): *Tectonophysics*, p. 37-54, doi: 10.1016/j.tecto.2004.10.017
- Allen, J. L., 2004, Timing, Style, and Significance of Cambrian through Laramide brittle reactivation along the Proterozoic Homestake Shear zone, Colorado Mineral Belt: *Rocky Mountain Geology*, v. 39, no. 2, p. 65-84
- Allen, J. L., Shaw, C. A., 2013, Seismogenic fault-zone processes and heterogeneity recorded by pseudotachylyte: New insights from the Homestake Shear Zone, Colorado: *Geological Society of America Field Guide* 33, p. 165-183, doi: 10.1130/2013.0033(05)
- Allen, J. L., O'Hara, K.D., Moecher D.P., 2002, Structural Geometry and Thermal history of pseudotachylyte from the Homestake Shear Zone, Sawatch Range, Colorado: *Geological Society of America Field Guides*, p. 17-32, doi: 10.1130/0-8137-0003-5.17
- Amato, J. M., Boullion, A. O., Serna, A. M., Sanders, A. E., Farmer, G. L., Gehrels, G. E., Wooden, J. L., 2008, Evolution of the Mazatzal province and the timing of the Mazatzal orogeny: Insights from U-Pb geochronology and geochemistry of igneous and metasedimentary rocks in southern New Mexico: *GSA Bulletin*; v.120, no.3/4, p. 328-346, doi: 10.1130/B26200.1
- Blakey, R., Colorado Plateau Geosystems Inc., Paleogeography and Geologic Evolution of North America: <http://cpgeosystems.com/nam.html> (accessed October 2015).
- Brainerd, A.E., Baldwin Jr., H. L., Keyte, I. A., 1933, Pre-Pennsylvanian Stratigraphy of the Front Range in Colorado: *Bulletin of the American Association of Petroleum Geologists*; v. 17, no. 4, p. 375-396
- Caine, J. S., Nelson, E. P., Beach, S. T., Layer, P. W., 2006, Structural Fabrics, Mineralization, and Laramide Kinematics of the Idaho Springs-Ralston Shear Zone, Colorado Mineral Belt and the Central Front Range Uplift: *The Mountain Geologist*; v. 43, no. 1, p. 1-24

- Chapin, C. E., 2012, Origin of the Colorado Mineral Belt: *Geosphere*, v. 8, no. 1, p. 28-43, doi: 10.1130/GES00694.1
- Chapin, C. E., Cather, S. M., 1994, Tectonic Setting of the Axial Basins of the Northern and Central Rio Grande Rift: *Geological Society of America Special Paper*, v. 291, p. 5-25
- Chapin, C. E., Kelley, S. A., Cather, S. M., 2014, The Rocky Mountain Front, Southwestern USA: *Geosphere*, v. 10, no. 5, p. 1043–1060, doi:10.1130/GES01003.1
- Curtis, G. R., 1997, The Colorado Mineral Belt, *Rocky Mountain Association of Geologists Colorado Front Range Guidebook*, p. 77-84
- Fossen, H., 2010, *Structural Geology*: New York, Cambridge University Press, 463 p.
- Jones, J. V. III, Connelly, J. N., Karlstrom, K. E., Williams, M. L., Doe, M. F., 2009, Age, provenance, and tectonic setting of Paleoproterozoic quartzite successions the southwestern United States: *GSA Bulletin*, v. 121, no. 1/2, p. 247-264, doi: 10.1130/B26351.1
- Karlstrom, K. E., Humphreys, E. D., 1998, Persistent influence of Proterozoic accretionary boundaries in the tectonic evolution of southwestern North America: Interaction of tectonic grain and mantle modification events: *Rocky Mountain Geology*, v. 33, no. 2, p. 161-179
- Kellogg, K. S., Bryant, B., Reed, J. C., 2004, The Colorado Front Range - Anatomy of a Laramide Uplift: *Geological Society of America Field Guide 5*, p. 89-108
- Kelly, S., Chamberlin, R., 2012, Our Growing Understanding of the Rio Grande Rift: *New Mexico Earth Matters*, v. 12, p. 1-4
- Kirkham, R. M., Houck, K. J., Funk, J., Mendel, D., Sicard, K. R., 2012, Minturn Quadrangle Geologic Map, Eagle County, Colorado: Colorado Geological Survey, scale 1: 24,000
- Kirkham, R. M., Houck, K. J., Funk, J., Mendel, D., Sicard, K. R., 2011, Open File Report 12-08: Minturn Quadrangle Geologic Map, Eagle County, Colorado, p. 1-57
- Kluth, C. F., 1986, *Plate Tectonics of the Ancestral Rocky Mountains*: AAPG

Memoir, v. 41, p. 353- 369

Lee, P. E., Jessup, M. J., Shaw, C. A., Hicks, G. L., Allen, J. L., 2012, Strain Partitioning in the mid-crust of a transpressional shear zone system: Insights from the Homestake and Slide Lake shear zones, central Colorado: *Journal of Structural Geology*, v. 39, p. 237-252, doi 10.1016/j.jsg.201202.006

Lovering, T. S., Tweto, O., Lovering, T. G., 1978, Ore Deposits of the Gilman District, Eagle County Colorado: Geological Survey Professional Paper 1017, p. 1-90

Matthews, V., KellerLynn, K. and Fox, B., 2009, Messages in Stone: Colorado's Colorful Geology: Denver, Colorado Geological Survey, 163 p.

Murphy, J. A., 2002, Preserving Mineral and Mining History at the Eagle Mine: *Rocks & Minerals*, p. 324 -328

Myrow, P. M., Taylor, J. F., Miller, J. F., Ethington, R. L., Ripperdan, R. L., Allen, J., 2003, Fallen Arches: Dispelling myths concerning Cambrian and Ordovician paleogeography of the Rocky Mountain region: *GSA Bulletin*, v. 115, no. 6, p. 695-713

Nesse, W. D., 2006, Geometry and Tectonics of the Laramide Front Range, Colorado: *The Mountain Geologist*, v. 43, no. 1, p. 25-44

Reed, J., Ellis G., 2009, *Rocks Above the Clouds: A Hiker's and Climber's Guide to Colorado Mountain Geology*, Golden, Colorado, The Colorado Mountain Club Press, p. 130-144

Shaw, C. A., Allen, J. L., 2007, Field Rheology and Structural Evolution of the Homestake Shear Zone, Colorado: *Rocky Mountain Geology*, v. 42, no. 1, p. 31-56

Sims, P. K., 2009, The Trans-Rocky Mountain Fault System-A Fundamental Precambrian Strike-Slip System: U.S. Geological Survey Circular 1334, p. 13

Stone, D. S., 2002, Morphology of the Casper Mountain uplift and related, subsidiary structures, central Wyoming: Implications for Laramide kinematics, dynamics, and crustal inheritance: *AAPG Bulletin*, v. 86, no. 8, p. 1417-1440

- Tweto, O., 1975, Laramide (Late Cretaceous-Early Tertiary) Orogeny in the Southern Rocky Mountains: Geological Society of America Memoir, p. 1-44
- Tweto, O., 1980, Precambrian Geology of Colorado: Rocky Mountain Association of Geologists 1980 symposium, p. 37-46
- Tweto, O., 1989, Rock Units of the Precambrian Basement in Colorado: U.S. Geological Survey Professional Paper 1321-A: Washington, United States Government Printing Office, p. 1-59
- Tweto, O., 1980, Summary of Laramide Orogeny in Colorado: Rocky Mountain Association of Geologists 1980 symposium, p. 129-134
- Tweto, O., 1977, Tectonic History of West-Central Colorado: Rocky Mountain Association of Geologists 1977 symposium, p. 11-22
- Tweto, O., Case, J. E., 1972, Gravity and Magnetic Features as Related to Geology in the Leadville 30-Minute Quadrangle, Colorado, Geological Survey Professional Paper 726 C: Washington, United States Government Printing Office, p. 1-31
- Tweto, O., Lovering, T. S., 1977, Geology of the Minturn 15-Minute Quadrangle, Eagle and Summit Counties, Colorado: Geological Survey Professional Paper 956, p. 1-99
- Weil, A. B., Yonkee, A., Schultz, M., 2016, Tectonic evolution of a Laramide transverse structural zone: Sweetwater Arch, south central Wyoming: *Tectonics*, p. 1090-1120, doi:10.1002/2016TC004122
- Whitmeyer, S. J., Karlstrom, K. E., 2007, Tectonic Model for the Proterozoic Growth of North America: *Geosphere*, v. 3, no. 4, p. 220-259, doi: 10.1130/GES00055.1

APPENDIX

Planar Data

Locality		ID	Latitude	Longitude	Plane Type	Strike	Dip	Unit
Name								
2		1	39.5083	-106.3756	Joint	55	74	Diorite
2		2	39.5083	-106.3756	Joint	140	74	Diorite
2		3	39.5083	-106.3756	Fault	37	65	Diorite
2		4	39.5083	-106.3756	Joint	260	24	Diorite
2		5	39.5083	-106.3756	Joint	12	55	Diorite
2		6	39.5083	-106.3756	Joint	78	70	Diorite
2		7	39.5083	-106.3756	Joint	56	68	Diorite
2		8	39.5083	-106.3756	Joint	100	56	Diorite
2		9	39.5083	-106.3758	Fault	37	65	Diorite
3		10	39.5077	-106.3792	Joint	30	81	Diorite
3		11	39.5077	-106.3792	Joint	329	15	Diorite
3		12	39.5077	-106.3792	Joint	10	75	Diorite
3		13	39.5077	-106.3792	Joint	222	63	Diorite
3		14	39.5077	-106.3792	Joint	355	90	Diorite
3		15	39.5077	-106.3792	Joint	25	29	Diorite
3		16	39.5077	-106.3792	Joint	287	72	Diorite
3		17	39.5078	-106.3792	Fault	285	85	Diorite
4		18	39.5078	-106.3799	Fault	45	71	Diorite
5		19	39.5079	-106.3802	Joint	159	69	Diorite
5		20	39.5079	-106.3802	Joint	159	90	Diorite
5		21	39.5079	-106.3802	Joint	334	23	Diorite
5		22	39.5079	-106.3802	Joint	56	86	Diorite
6		23	39.5083	-106.3806	Joint	53	89	Diorite
6		24	39.5084	-106.3798	Fault	194	65	Diorite
6		25	39.5091	-106.3818	Fault	341	15	Diorite
7		26	39.5074	-106.3774	Foliation	279	73	Diorite
7		27	39.5074	-106.3774	Fault	80	66	Diorite
7		28	39.5074	-106.3774	Fault	66	58	Diorite
7		29	39.5075	-106.3773	Fault	131	58	Diorite

7	30	39.5075	-106.3773	Joint	17	90	Diorite
7	31	39.5075	-106.3773	Joint	152	68	Diorite
7	32	39.5075	-106.3773	Joint	266	90	Diorite
7	33	39.5075	-106.3773	Joint	307	19	Diorite
7	34	39.5073	-106.3775	Fault	83	88	Gneiss
7	35	39.5073	-106.3773	Fault	348	25	Cross Creek Granite
7	36	39.5073	-106.3776	Fault	318	72	Cross Creek Granite
7	37	39.5073	-106.3776	Foliation	93	75	Cross Creek Granite
7	38	39.5071	-106.3777	Foliation	103	79	Cross Creek Granite
7	39	39.5074	-106.3773	Fault	72	71	Gneiss
7	40	39.5065	-106.3780	Foliation	70	65	Gneiss
8	41	39.5091	-106.3764	Fault	35	74	Sawatch Formation
9	42	39.5094	-106.3765	Fault	195	85	Sawatch Formation
9	43	39.5094	-106.3765	Fault	4	65	Sawatch Formation
9	44	39.5094	-106.3765	Fault	357	77	Sawatch Formation
9	45	39.5094	-106.3765	Fault	17	74	Sawatch Formation
9	46	39.5094	-106.3765	Fault	22	90	Sawatch Formation
9	47	39.5094	-106.3765	Fault	208	74	Sawatch Formation
10	48	39.5088	-106.3765	Bedding	272	4	Sawatch Formation
10	49	39.5096	-106.3775	Fault	63	74	Sawatch Formation
11	50	39.5084	-106.3816	Joint	257	30	Diorite
11	51	39.5085	-106.3816	Joint	60	61	Diorite
12	52	39.5085	-106.3826	Fault	47	61	Diorite
12	53	39.5084	-106.3816	Joint	241	8	Diorite
12	54	39.5084	-106.3816	Joint	120	90	Diorite
12	55	39.5084	-106.3816	Joint	28	76	Diorite

12	56	39.5084	-106.3816	Joint	77	90	Diorite
13	57	39.5093	-106.3836	Joint	151	74	Diorite
13	58	39.5093	-106.3836	Joint	322	14	Diorite
13	59	39.5093	-106.3836	Joint	272	81	Diorite
13	60	39.5092	-106.3837	Joint	150	76	Diorite
15	61	39.5101	-106.3842	Joint	215	79	Diorite
15	62	39.5101	-106.3842	Joint	210	42	Diorite
15	63	39.5101	-106.3842	Joint	9	55	Diorite
15	64	39.5100	-106.3841	Joint	169	84	Diorite
15	65	39.5099	-106.3844	Fault	233	59	Diorite
16	66	39.5125	-106.3845	Joint	147	71	Gneiss
16	67	39.5125	-106.3845	Joint	25	87	Gneiss
16	68	39.5125	-106.3845	Joint	269	14	Gneiss
16	69	39.5125	-106.3845	Foliation	42	80	Gneiss
16	70	39.5646	-106.4144	Foliation	256	77	Gneiss
16	71	39.5646	-106.4144	Joint	74	41	Gneiss
16	72	39.5646	-106.4144	Joint	221	67	Gneiss
16	73	39.5646	-106.4144	Joint	153	83	Gneiss
16	74	39.5116	-106.3845	Joint	90	88	Diorite
16	75	39.5118	-106.3840	Joint	350	12	Diorite
16	76	39.5116	-106.3843	Foliation	316	80	Diorite
							Cross Creek
20	77	39.5130	-106.3853	Joint	50	79	Granite
							Cross Creek
20	78	39.5130	-106.3851	Joint	56	43	Granite
							Cross Creek
20	79	39.5130	-106.3849	Fault	25	53	Granite
							Cross Creek
20	80	39.5130	-106.3849	Joint	249	65	Granite
21	81	39.5142	-106.3866	Fault	193	26	Diorite
21	82	39.5142	-106.3866	Fault	210	41	Diorite
21	83	39.5142	-106.3866	Fault	285	39	Diorite
21	84	39.5143	-106.3863	Fault	228	73	Diorite
21	85	39.5142	-106.3869	Fault	205	59	Diorite
21	86	39.5141	-106.3866	Fault	214	47	Diorite
21	87	39.5142	-106.3864	Joint	14	19	Diorite
21	88	39.5142	-106.3864	Joint	144	89	Diorite

21	89	39.5142	-106.3864	Joint	231	81	Diorite
22	90	39.5144	-106.3869	Fault	27	72	Cross Creek Granite
22	91	39.5144	-106.3869	Fault	60	54	Cross Creek Granite
23	92	39.5149	-106.3874	Fault	36	62	Gneiss
23	93	39.5149	-106.3874	Joint	184	55	Gneiss
23	94	39.5149	-106.3874	Joint	46	47	Gneiss
23	95	39.5149	-106.3874	Joint	204	68	Gneiss
23	96	39.5149	-106.3874	Joint	149	29	Gneiss
23	97	39.5149	-106.3874	Joint	149	36	Gneiss
23	98	39.5148	-106.3873	Fault	55	51	Gneiss
25	99	39.5157	-106.3886	Fault	50	90	Gneiss
26	100	39.5152	-106.3877	Joint	147	84	Gneiss
26	101	39.5152	-106.3877	Joint	48	54	Gneiss
26	102	39.5152	-106.3877	Joint	221	5	Gneiss
26	103	39.5152	-106.3877	Fault	36	66	Gneiss
27	104	39.5160	-106.3891	Fault	43	58	Gneiss
29	105	39.5166	-106.3907	Joint	84	47	Diorite
29	106	39.5166	-106.3907	Joint	283	14	Diorite
29	107	39.5166	-106.3907	Joint	228	62	Diorite
29	108	39.5166	-106.3907	Joint	150	77	Diorite
30	109	39.5166	-106.3913	Fault	50	75	Gneiss
30	110	39.5166	-106.3913	Foliation	321	81	Gneiss
32	111	39.5175	-106.3921	Fault	141	54	Gneiss
32	112	39.5173	-106.3919	Fault	168	84	Gneiss
33	113	39.5166	-106.3939	Joint	256	30	Cross Creek Granite
33	114	39.5166	-106.3939	Joint	69	73	Cross Creek Granite
33	115	39.5166	-106.3939	Joint	130	66	Cross Creek Granite
33	116	39.5166	-106.3939	Fault	49	57	Cross Creek Granite
33	117	39.5163	-106.3941	Fault	58	43	Cross Creek Granite
34	118	39.5180	-106.3940	Joint	49	15	Gneiss
34	119	39.5180	-106.3940	Joint	135	66	Gneiss

34	120	39.5180	-106.3940	Joint	50	82	Gneiss
34	121	39.5180	-106.3943	Fault	41	71	Gneiss
35	122	39.5184	-106.3944	Joint	55	64	Gneiss
35	123	39.5184	-106.3941	Joint	181	82	Gneiss
35	124	39.5184	-106.3941	Joint	348	10	Gneiss
35	125	39.5630	-106.4134	Joint	164	72	Gneiss
35	126	39.5571	-106.4111	Joint	219	53	Gneiss
35	127	39.5185	-106.3945	Joint	40	66	Gneiss
35	128	39.5185	-106.3945	Fault	164	54	Gneiss
36	129	39.5193	-106.3944	Joint	180	87	Cross Creek Granite
36	130	39.5194	-106.3944	Joint	150	76	Cross Creek Granite
36	131	39.5184	-106.3947	Fault	46	64	Cross Creek Granite
38	132	39.5238	-106.3961	Joint	132	35	Diorite
38	133	39.5238	-106.3961	Joint	229	3	Diorite
38	134	39.5238	-106.3961	Joint	219	89	Cross Creek Granite
38	135	39.5197	-106.3956	Fault	71	64	Diorite
39	136	39.5239	-106.3960	Joint	64	75	Cross Creek Granite
39	137	39.5239	-106.3960	Joint	35	1	Cross Creek Granite
39	138	39.5239	-106.3960	Joint	145	80	Cross Creek Granite
39	139	39.5630	-106.4136	Fault	223	45	Cross Creek Granite
40	140	39.5240	-106.3957	Joint	226	5	Cross Creek Granite
40	141	39.5239	-106.3956	Joint	222	69	Cross Creek Granite
40	142	39.5239	-106.3956	Joint	339	84	Cross Creek Granite
40	143	39.5240	-106.3958	Fault	239	48	Cross Creek Granite
41	144	39.5584	-106.4115	Fault	71	79	Cross Creek Granite

42	145	39.5584	-106.4115	Fault	145	21	Cross Creek Granite
42	146	39.5584	-106.4115	Joint	55	51	Cross Creek Granite
44	147	39.5271	-106.4004	Joint	47	79	Cross Creek Granite
44	148	39.5271	-106.4004	Joint	52	59	Cross Creek Granite
44	149	39.5271	-106.4004	Joint	50	72	Cross Creek Granite
44	150	39.5273	-106.4001	Joint	298	27	Cross Creek Granite
44	151	39.5273	-106.4001	Joint	261	70	Cross Creek Granite
44	152	39.5273	-106.4001	Joint	62	69	Cross Creek Granite
44	153	39.5273	-106.4001	Joint	145	75	Cross Creek Granite
45	154	39.5284	-106.4012	Joint	223	83	Cross Creek Granite
45	155	39.5281	-106.4008	Joint	50	80	Cross Creek Granite
45	156	39.5281	-106.4008	Joint	291	85	Cross Creek Granite
45	157	39.5282	-106.4009	Fault	77	47	Cross Creek Granite
45	158	39.5285	-106.4009	Joint	163	79	Cross Creek Granite
45	159	39.5286	-106.4010	Joint	282	6	Cross Creek Granite
45	160	39.5280	-106.4014	Joint	50	80	Cross Creek Granite
45	161	39.5280	-106.4017	Joint	291	85	Cross Creek Granite
46	162	39.5088	-106.3764	Bedding	313	1	Sawatch Formation
46	163	39.5088	-106.3760	Bedding	335	7	Sawatch Formation
46	164	39.5088	-106.3760	Joint	140	79	Sawatch Formation

46	165	39.5088	-106.3760	Joint	52	75	Sawatch Formation
47	166	39.5088	-106.3765	Bedding	129	14	Sawatch Formation
48	167	39.5096	-106.3782	Fault	104	53	Sawatch Formation
48	168	39.5096	-106.3783	Fault	95	38	Sawatch Formation
48	169	39.5096	-106.3783	Joint	147	77	Sawatch Formation
48	170	39.5096	-106.3783	Joint	235	82	Sawatch Formation
48	171	39.5096	-106.3783	Bedding	15	5	Sawatch Formation
49	172	39.5090	-106.3806	Bedding	324	30	Sawatch Formation
49	173	39.5091	-106.3797	Bedding	278	18	Sawatch Formation
49	174	39.5091	-106.3797	Joint	125	78	Sawatch Formation
49	175	39.5089	-106.3795	Joint	24	90	Sawatch Formation
50	176	39.5095	-106.3804	Bedding	275	36	Sawatch Formation
50	177	39.5095	-106.3804	Fault	88	69	Sawatch Formation
51	178	39.5099	-106.3808	Joint	113	65	Sawatch Formation
51	179	39.5099	-106.3808	Joint	63	88	Sawatch Formation
51	180	39.5100	-106.3808	Bedding	301	24	Sawatch Formation
52	181	39.5103	-106.3829	Bedding	253	12	Sawatch Formation
52	182	39.5103	-106.3829	Joint	141	84	Sawatch Formation
52	183	39.5103	-106.3829	Joint	49	90	Sawatch Formation
53	184	39.5103	-106.3829	Joint	120	79	Sawatch Formation

53	185	39.5103	-106.3829	Joint	205	90	Sawatch Formation
53	186	39.5105	-106.3827	Bedding	350	14	Sawatch Formation
54	187	39.5116	-106.3826	Joint	95	61	Sawatch Formation
54	188	39.5116	-106.3826	Joint	126	67	Sawatch Formation
54	189	39.5116	-106.3826	Bedding	352	11	Sawatch Formation
55	190	39.5119	-106.3826	Fault	206	73	Sawatch Formation
56	191	39.5127	-106.3827	Joint	220	83	Sawatch Formation
56	192	39.5127	-106.3827	Joint	134	68	Sawatch Formation
56	193	39.5127	-106.3827	Bedding	338	16	Sawatch Formation
58	194	39.5132	-106.3834	Joint	35	77	Sawatch Formation
58	195	39.5134	-106.3836	Joint	176	33	Sawatch Formation
58	196	39.5134	-106.3836	Bedding	296	3	Sawatch Formation
58	197	39.5134	-106.3836	Joint	237	80	Sawatch Formation
58	198	39.5471	-106.4025	Joint	188	60	Sawatch Formation
60	199	39.5147	-106.3849	Joint	63	89	Sawatch Formation
60	200	39.5147	-106.3849	Joint	21	90	Sawatch Formation
60	201	39.5147	-106.3849	Joint	118	43	Sawatch Formation
60	202	39.5147	-106.3849	Joint	285	81	Sawatch Formation
60	203	39.5147	-106.3847	Joint	308	90	Sawatch Formation
60	204	39.5147	-106.3847	Joint	228	88	Sawatch Formation

60	205	39.5146	-106.3849	Bedding	300	10	Sawatch Formation
61	206	39.5147	-106.3844	Bedding	310	15	Sawatch Formation
61	207	39.5147	-106.3845	Fault	58	55	Sawatch Formation
62	208	39.5148	-106.3846	Joint	218	69	Sawatch Formation
62	209	39.5148	-106.3846	Joint	353	70	Sawatch Formation
62	210	39.5147	-106.3845	Fault	154	78	Sawatch Formation
63	211	39.5148	-106.3846	Fault	308	90	Sawatch Formation
64	212	39.5147	-106.3847	Joint	178	32	Sawatch Formation
64	213	39.5147	-106.3847	Joint	221	79	Sawatch Formation
64	214	39.5148	-106.3847	Joint	40	77	Sawatch Formation
65	215	39.5144	-106.3847	Joint	128	39	Sawatch Formation
65	216	39.5144	-106.3847	Joint	206	80	Sawatch Formation
65	217	39.5145	-106.3847	Fault	328	47	Sawatch Formation
66	218	39.5110	-106.3826	Bedding	300	4	Sawatch Formation
66	219	39.5110	-106.3825	Joint	231	89	Sawatch Formation
66	220	39.5110	-106.3825	Joint	135	78	Sawatch Formation
67	221	39.5107	-106.3828	Joint	132	65	Sawatch Formation
67	222	39.5107	-106.3828	Joint	62	84	Sawatch Formation
67	223	39.5107	-106.3828	Bedding	315	15	Sawatch Formation
68	224	39.5103	-106.3829	Joint	119	80	Sawatch Formation

68	225	39.5103	-106.3829	Joint	251	90	Sawatch Formation
68	226	39.5103	-106.3829	Joint	205	80	Sawatch Formation
69	227	39.5098	-106.3818	Joint	244	88	Sawatch Formation
69	228	39.5098	-106.3818	Joint	287	76	Sawatch Formation
69	229	39.5098	-106.3818	Bedding	261	17	Sawatch Formation
69	230	39.5099	-106.3822	Bedding	326	9	Sawatch Formation
69	231	39.5100	-106.3822	Joint	319	90	Sawatch Formation
69	232	39.5100	-106.3822	Joint	204	84	Sawatch Formation
70	233	39.5097	-106.3812	Joint	204	79	Sawatch Formation
70	234	39.5096	-106.3813	Joint	118	71	Sawatch Formation
71	235	39.5092	-106.3790	Bedding	211	17	Sawatch Formation
71	236	39.5092	-106.3790	Joint	116	77	Sawatch Formation
71	237	39.5092	-106.3791	Joint	70	83	Sawatch Formation
72	238	39.5093	-106.3789	Joint	33	75	Sawatch Formation
72	239	39.5093	-106.3789	Joint	106	90	Sawatch Formation
72	240	39.5093	-106.3789	Bedding	350	16	Sawatch Formation
73	241	39.5097	-106.3808	Fault	254	90	Sawatch Formation
74	242	39.5097	-106.3807	Bedding	301	24	Sawatch Formation
74	243	39.5097	-106.3807	Bedding	246	12	Sawatch Formation

Linear Data

Locality	ID	Latitude	Longitude	Lineation Type	Plunge	Bearing	Unit
2	1	39.5083	-106.3756	Slickenside	69	158	Diorite
2	2	39.5083	-106.3756	Slickenside	65	120	Diorite
6	3	39.5085	-106.3800	Slickenside	0	195	Diorite
6	4	39.5091	-106.3819	Slickenside	14	55	Diorite
7	5	39.5075	-106.3773	Slickenside	56	261	Diorite
7	6	39.5073	-106.3775	Slickenside	25	81	Gneiss Cross Creek
7	7	39.5073	-106.3773	Slickenside	80	20	Granite Cross Creek
7	8	39.5073	-106.3776	Slickenside	72	55	Granite
7	9	39.5074	-106.3773	Slickenside	48	100	Gneiss
7	10	39.5065	-106.3780	Lineation	60	162	Gneiss Sawatch Formation
8	11	39.5091	-106.3765	Slickenside	5	31	Gneiss
12	12	39.5084	-106.3825	Slickenside	54	200	Diorite
15	13	39.5099	-106.3844	Slickenside	4	240	Diorite
21	14	39.5142	-106.3866	Slickenside	20	276	Diorite
21	15	39.5142	-106.3866	Slickenside	41	279	Diorite
21	16	39.5142	-106.3866	Slickenside	14	275	Diorite
21	17	39.5143	-106.3863	Slickenside	10	224	Diorite
21	18	39.5141	-106.3868	Slickenside	14	200	Diorite
21	19	39.5141	-106.3866	Slickenside	44	270	Diorite
23	20	39.5149	-106.3874	Slickenside	11	19	Gneiss
27	21	39.5160	-106.3891	Slickenside	1	37	Gneiss
30	22	39.5166	-106.3913	Slickenside	73	155	Gneiss
30	23	39.5166	-106.3913	Lineation	80	335	Gneiss
32	24	39.5175	-106.3921	Slickenside	40	175	Gneiss
32	25	39.5173	-106.3919	Slickenside	6	172	Gneiss Cross Creek
33	26	39.5166	-106.3939	Slickenside	13	31	Granite
35	27	39.5185	-106.3945	Slickenside	51	60	Gneiss

							Cross Creek
36	28	39.5184	-106.3947	Slickenside	63	139	Granite
38	29	39.5197	-106.3956	Slickenside	4	58	Diorite
							Cross Creek
39	30	39.5630	-106.4136	Slickenside	40	300	Granite
							Cross Creek
40	31	39.5240	-106.3958	Slickenside	44	319	Granite
							Cross Creek
41	32	39.5584	-106.4115	Slickenside	78	169	Granite
							Cross Creek
45	33	39.5282	-106.4009	Slickenside	58	138	Granite
							Sawatch
48	34	39.5096	-106.3782	Slickenside	1	296	Formation
							Sawatch
48	35	39.5096	-106.3783	Slickenside	3	281	Formation
							Sawatch
50	36	39.5095	-106.3804	Slickenside	1	267	Formation
							Sawatch
55	37	39.5119	-106.3826	Slickenside	11	209	Formation
							Sawatch
61	38	39.5147	-106.3845	Slickenside	32	169	Formation
							Sawatch
62	39	39.5147	-106.3845	Slickenside	6	168	Formation
							Sawatch
63	40	39.5148	-106.3846	Slickenside	7	305	Formation

VITA

Kaitlin Lee Askelson grew up in Indian Hills, Colorado and attended Conifer High School in Conifer, Colorado. After graduating in 2008, Kaitlin attended Fort Lewis College in Durango, Colorado. While at Fort Lewis College, Kaitlin conducted research titled “Geometric and Kinematic Modeling of the Rampart Range Fault, Colorado Springs, Colorado” with Dr. Kim Hannula. In April 2013, she graduated Cum Laude and received a Bachelor of Science with a major in Geology- Environmental Option and an Art minor from Fort Lewis College. After graduation, Kaitlin worked in the oil and gas industry conducting geosteering and remote logging of wells. In August 2015, she began graduate school at Stephen F. Austin State University and taught Geology 101 and Geology 132 labs as a Graduate Teaching Assistant. Kaitlin received her Master of Science degree from Stephen F. Austin State University in May 2017.

Permanent Address: 22928 Pawnee Rd.
P.O. Box 758
Indian Hills, CO 80454

GSA style guide

This thesis was typed by Kaitlin Lee Askelson